ACS Infectious Diseases

pubs.acs.org/journal/aidcbc Article

Comparative Multiplexed Interactomics of SARS-CoV-2 and Homologous Coronavirus Nonstructural Proteins Identifies Unique and Shared Host-Cell Dependencies

Jonathan P. Davies,[‖] Katherine M. Almasy,[‖] Eli F. McDonald, and Lars Plate*

Cite This: *ACS Infect. Dis.* 2020, 6, 3174−3189 Read Online

ACCESS | Metrics & More | Article Recommendations | Supporting Information

ABSTRACT: Human coronaviruses (hCoVs) have become a threat to global health and society, as evident from the SARS outbreak in 2002 caused by SARS-CoV-1 and the most recent COVID-19 pandemic caused by SARS-CoV-2. Despite a high sequence similarity between SARS-CoV-1 and -2, each strain has a distinctive virulence. A better understanding of the basic molecular mechanisms mediating changes in virulence is needed. Here, we profile the virus-host protein−protein interactions of two hCoV nonstructural proteins (nsps) that are critical for virus replication. We use tandem mass tag-multiplexed quantitative proteomics to sensitively compare and contrast the interactomes of nsp2 and nsp4 from three betacoronavirus strains: SARS-CoV-1, SARS-CoV-2, and hCoV-OC43—an endemic strain associated with the common cold. This approach enables the identification of both unique and shared host cell protein binding partners and the ability to further compare the enrichment of common interactions across homologues from related strains. We identify common nsp2 interactors involved in endoplasmic reticulum (ER) Ca^{2+} signaling and mitochondria biogenesis. We also identify nsp4 interactors unique to each strain, such as E3 ubiquitin ligase complexes for SARS-CoV-1 and ER homeostasis factors for SARS-CoV-2. Common nsp4 interactors include *N*-linked glycosylation machinery, unfolded protein response associated proteins, and antiviral innate immune signaling factors. Both nsp2 and nsp4 interactors are strongly enriched in proteins localized at mitochondria-associated ER membranes suggesting a new functional role for modulating host processes, such as calcium homeostasis, at these organelle contact sites. Our results shed light on the role these hCoV proteins play in the infection cycle, as well as host factors that may mediate the divergent pathogenesis of OC43 from SARS strains. Our mass spectrometry workflow enables rapid and robust comparisons of multiple bait proteins, which can be applied to additional viral proteins. Furthermore, the identified common interactions may present new targets for exploration by host-directed antiviral therapeutics.

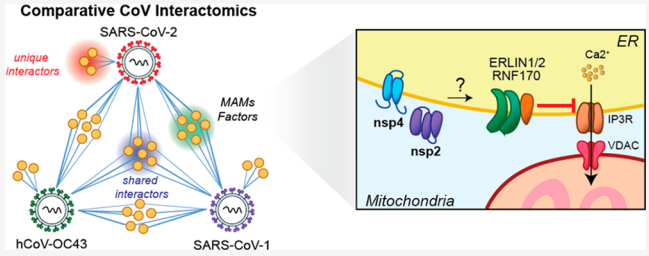

KEYWORDS: *affinity purification-mass spectrometry, tandem mass tags, COVID-19, nsp2, nsp4, mitochondria-associated endoplasmic reticulum membrane*

Coronaviruses (CoVs) are positive-strand RNA viruses capable of causing human disease with a range of severity. While some strains, such as endemic hCoV-OC43, cause milder common-cold like symptoms, other strains are associated with more severe pathogenesis and higher lethality, including SARS-CoV-1 (emerged in 2002), MERS-CoV (in 2012), and most recently SARS-CoV-2, the causative agent of COVID-19.[1,2] Despite the relevance of CoVs for human health, our understanding of the factors governing their divergent pathogenicity remains incomplete. Pathogenicity may be mediated by a variety of factors, including different specificities and affinity for different cell surface receptors such as angiotensin-converting enzyme 2 (ACE2) for SARS-CoV-1 and SARS-CoV-2[1,3] or 9-*O*-acetylated sialic acid for hCoV-OC43.[4] CoV strains also engage a variety of host immune processes in infected cells. Pathogenic strains more strongly interfere with interferon I signaling[4,5] and induce apoptosis and pyroptosis.[6−9] Ensembles of virus-host protein−protein interactions (PPIs) orchestrate the reprogramming of these processes during infection.

Coronaviruses possess the largest known RNA viral genomes, ∼30 kbp in length. The 5′ 20 kb region of the genome encodes for two open reading frames (orf1*a*/1*ab*) that produce 16 nonstructural proteins (nsp1−nsp16) needed to form the viral replication complex, while the 3′ proximal region encodes for the structural proteins and several accessory

Received: July 14, 2020
Published: December 2, 2020

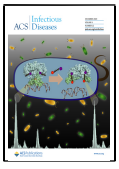

https://dx.doi.org/10.1021/acsinfecdis.0c00500
ACS Infect. Dis. 2020, 6, 3174−3189

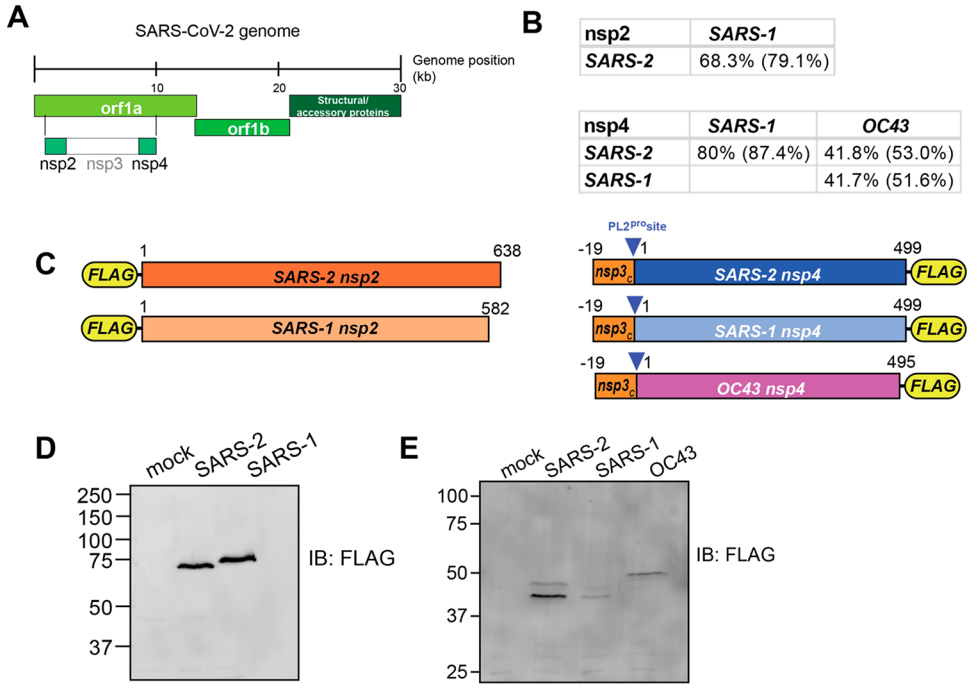

Figure 1. Design and validation of expression of CoV nsp2 and nsp4 constructs for affinity purification. (A) Schematic of SARS-CoV-2 genome organization. (B) Amino acid sequence identity and similarity (in parentheses) for comparisons of nsp2 and nsp4 homologues. Sequence alignments are shown in Figure S1A,B. (C) Nsp2 and nsp4 FLAG-tagged construct designs. Nsp2 constructs contain a N-terminal FLAG-tag. Nsp4 constructs contain a 19 amino acid leader sequence from nsp3 at the N-terminus, including the $PL2^{pro}$ cleavage site, along with a C-terminal FLAG-tag. (D, E) Western blot of nsp2 and nsp4 homologues expressed in HEK293T cells. Cells were transiently transfected with FLAG-nsp2 (D) or nsp4-FLAG (E). Proteins were detected using an anti-FLAG antibody.

factors with varying roles (Figure 1A). Previous protein−protein interaction studies of individual CoV proteins have shed light on their functions in the infected host cells and putative roles during pathogenesis. Yeast-two hybrid studies of coronavirus proteins have identified intraviral interactions[10] and interactions between nsp1 and immunophilins,[11] and a proximity-labeling approach was used to determine the host proteins concentrated in sites of replication.[12]

Affinity purification-mass spectrometry (AP-MS) is a powerful tool to study virus-host interactions and has been used extensively to examine how viruses reorganize host cells.[13−16] A prior AP-MS study of SARS-CoV-1 nsp2 identified multiple host interactors including prohibitin 1/2 (PHB1/2).[17] Most notably, Gordon et al. recently profiled host interactors for 26 SARS-CoV-2 proteins.[18] While these studies enabled important insight on individual viral protein functions, they focused on single CoV strains, limiting direct cross-strain comparisons.

Here, we sought to profile and compare the host interaction profiles of nsps from multiple hCoVs, namely, hCoV-OC43, SARS-CoV-1, and SARS-CoV-2. Through comparative interactomics, we identify both conserved and unique interactors across various strains. Notably, a quantitative analysis of interaction enrichment enables a nuanced differentiation between shared interactions for each coronavirus protein. Through this approach we discovered both conserved and novel functions of viral proteins and the pathways by which they manipulate cellular processes. Comparisons across strains may also provide clues into the evolutionary arms race between virus and host proteins to hijack or protect protein−protein interfaces.[19] Additionally, identified host dependencies can potentially be exploited as targets for host-directed antiviral therapeutics.

In particular, we focus on the host interactors of nsp2 and nsp4. Nsp2 has been suggested to play a role in modifying the host cell environment, although its precise function remains unknown.[17] Nsp2 is dispensable for infection in SARS-CoV-1[20] and has pronounced amino acid sequence differences across coronavirus strains (Figures 1B and S1A). Additionally, an early sequence analysis of SARS-CoV-2 identified regions of positive selection pressure in nsp2.[21] Given the variability of sequence across strains and the ambiguous function, a comparison of interaction profiles across strains can yield insights into the role of nsp2. In contrast, the role of nsp4, a transmembrane glycoprotein, is better defined, most notably in the formation of the double-membrane vesicles associated with replication complexes.[22,23] Unlike nsp2, nsp4 has a high degree of sequence similarity across human coronavirus strains (Figures 1B and S1B).

In this study, we use affinity purification-proteomics to identify interactors of nsp2 from two human coronaviruses (SARS-CoV-1 and SARS-CoV-2) and interactors of nsp4 from three strains (OC43, SARS-CoV-1, and SARS-CoV-2). A quantitative comparative analysis of nsp2 interactors identifies common protein binding partners, including the ERLIN1/2 complex and prohibitin complex involved in regulation of mitochondrial function and calcium flux at endoplasmic reticulum (ER)-mitochondrial contact sites. We also identify overlapping nsp4 interactors, including N-linked glycosylation machinery, unfolded protein responsed (UPR) associated factors, and antiviral innate immune signaling proteins. Unique interactors of different nsp4 homologues include E3 ubiquitin ligase complexes for SARS-CoV-1 and ER homeostasis factors

https://dx.doi.org/10.1021/acsinfecdis.0c00500
ACS Infect. Dis. 2020, 6, 3174−3189

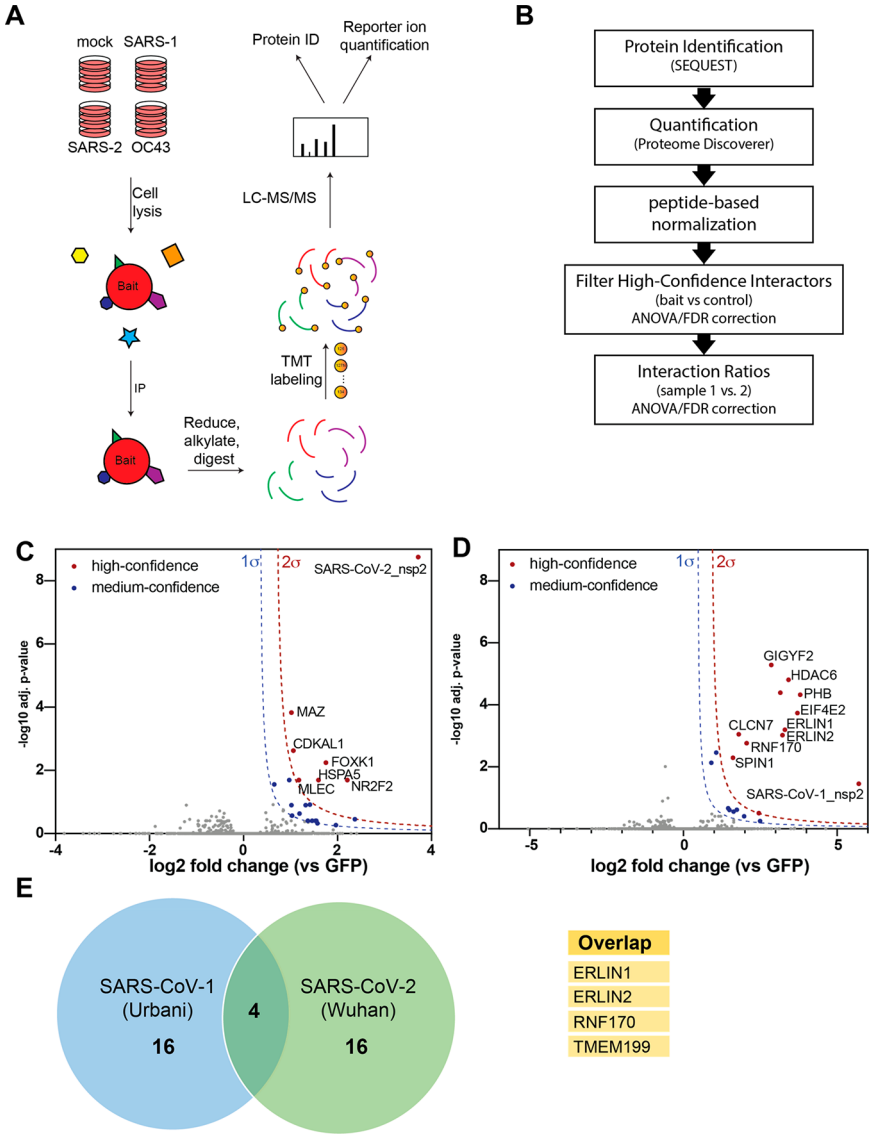

Figure 2. AP-MS identifies nsp2 interactors. (A) General AP-MS workflow to quantitatively determine interactors of viral nsp homologue. HEK293T cells are transfected with FLAG-tagged expression constructs of nsps as bait or GFP (mock) and lysed. Bait proteins are immunoprecipitated (IP) along with interacting proteins, reduced, alkylated, and tryptic-digested. Peptides are then tandem-mass tag (TMT) labeled, pooled, and analyzed by LC-MS/MS for identification and quantification. (B) Data processing workflow. Peptide spectra are identified and matched to corresponding proteins (SEQUEST HT), then quantified based on TMT reporter ion intensity (Proteome Discoverer 2.4). High confidence interactors are filtered by comparing bait vs control. Interaction ratios between bait homologues are determined (log2 fold change) and adjusted *p*-value calculated using ANOVA. (C, D) Volcano plot of SARS-CoV-2 nsp2 (C) and SARS-CoV-1 nsp2 (D) data sets to identify medium- and high-confidence interactors. Plotted are log2 TMT intensity fold changes for proteins between nsp2 bait channels and GFP mock transfections vs −log10 adjusted *p*-values. Curves for the variable cutoffs used to define high-confidence (red) or medium confidence (blue) interactors are shown. $1\sigma = 0.5$ for (C), $1\sigma = 0.43$ for (D). (E) Venn diagram comparing high-confidence interactors between nsp2 homologues. Sixteen unique proteins were identified each, while four proteins overlapped both data sets (listed in adjacent table).

for SARS-CoV-2. In particular, we found nsp2 and nsp4 interactors are strongly enriched for mitochondria-associated ER membranes (MAM) factors, suggesting a potential mechanism to affect calcium homeostasis and other host processes at these organelle contact sites.

RESULTS AND DISCUSSION

Design and Validation of Expression of CoV nsp2 and nsp4 Constructs for Affinity Purification. The two main open reading frames of the CoV viral genome, orf1*a* and orf1*ab*, encode for 16 nonstructural proteins, which perform a variety of tasks during the infection cycle (Figure 1A). We focus our analysis on two of these proteins, nsp2 and nsp4. Nsp2 is a less functionally well-understood protein with less than 70% amino acid sequence identity between the SARS-CoV-1 and SARS-CoV-2 homologues (Figures 1B and S1A). Nsp4 is a component of the CoV replication complex that is 80% identical between the SARS strains but only 42% identical between the SARS and OC43 strains, a less clinically severe human CoV (Figures 1B and S1B).

To compare the virus-host protein−protein interactions of nsp2 and nsp4 across multiple CoV strains, we designed FLAG-tagged expression constructs for affinity purification (Figure 1C). SARS-CoV-1 and SARS-CoV-2 nsp2 constructs

https://dx.doi.org/10.1021/acsinfecdis.0c00500
ACS Infect. Dis. 2020, 6, 3174−3189

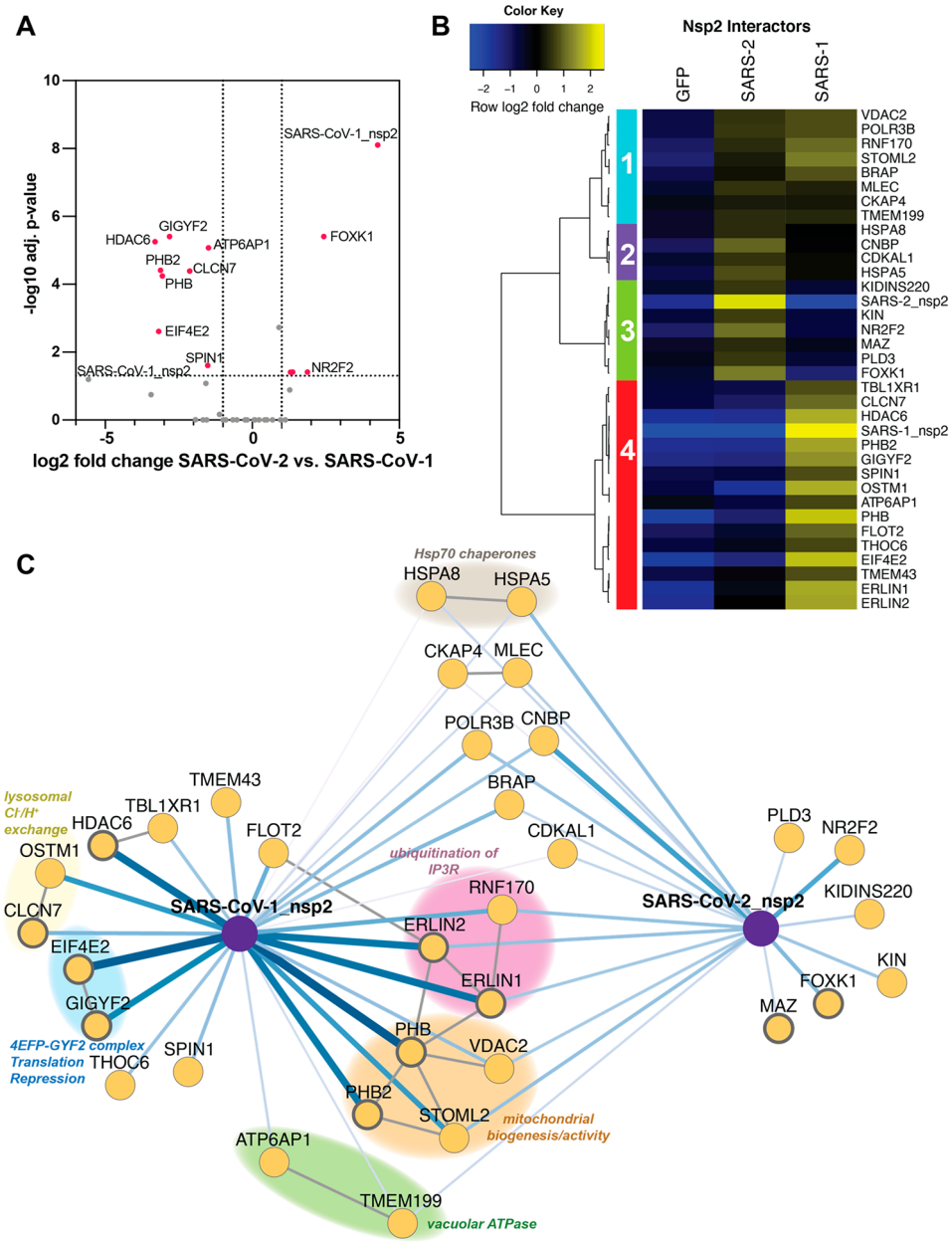

Figure 3. Quantitative comparison of SARS-CoV-1 and SARS-CoV-2 nsp2 interactors. (A) Volcano plot comparing interactions between an nsp2 homologue from SARS-CoV-1 and SARS-CoV-2. Only the high- and medium-confidence interactors of nsp2 are shown. Highlighted proteins meet the filter criteria of adjusted *p*-value < 0.05 and |log2 fold change| > 1. (B) Heatmap comparing the enrichment of SARS-CoV-1 and SARS-CoV-2 nsp2 interactors compared to GFP control. log2 fold change is color-coded and centered by row (blue low, yellow high enrichment). Hierarchical clustering using Ward's method shown on the left was performed on euclidean distances of log2 fold changes scaled by row. Clusters 1 and 2 correspond to shared interactors of SARS-CoV-1 and -2 nsp2, while clusters 3 and 4 are unique interactors for SARS-CoV-2 and SARS-CoV-1 nsp2, respectively. (C) Protein−Protein interaction (PPI) network map of nsp2 homologues. Blue lines indicate viral-host PPIs, where line width corresponds to fold enrichment compared to the GFP control. Gray lines indicate annotated host−host PPIs in STRING (score > 0.75). Groups of interactors with a common functional role are highlighted.

contain an N-terminal FLAG tag, while the SARS-CoV-1, SARS-CoV-2, and OC43 nsp4 constructs contain a C-terminal FLAG tag. In addition, nsp4 constructs contain a 19 amino acid leader sequence corresponding to the C-terminus of nsp3, which includes the nsp3-PL2^{pro} cleavage site necessary for proper nsp4 translocation into the ER membrane as has been shown previously.[24,25] Improper membrane insertion would likely alter the observed interactome as compared to the native state.

Protein constructs were transiently transfected into HEK293T cells, and proteins were detected by immunoblotting for the FLAG tag. While HEK293T cells are not representative of the primary physiological target tissue, these cells are permissive to infection and were able to recapitulate strong interactors expected in lung tissue in a prior SARS-CoV-2 interactome study.[18] The nsp2 constructs were detectable as a single protein band at the expected molecular weight (Figure 1D), while the nsp4 constructs displayed two distinct bands at a lower size than its expected molecular weight (Figure 1E).

https://dx.doi.org/10.1021/acsinfecdis.0c00500
ACS Infect. Dis. 2020, 6, 3174−3189

This lower apparent molecular weight was previously reported, and the different bands likely correspond to different glycosylation states.[18] To ensure nsp4 is expressed fully and the detected products do not correspond to a truncated protein, we immunopurified the protein using FLAG-agarose beads and analyzed the purified protein by liquid chromatography-mass spectrometry (LC-MS). We detected peptide fragments spanning the N- and C-termini with overall sequence coverage of up to 62% (Figure S1C−E) confirming expression of the full proteins.

Affinity Purification-Mass Spectrometry Identifies nsp2 Interactors. To identify host cell interaction partners of the distinct CoV nonstructural proteins, we employed an affinity purification-mass spectrometry workflow (Figure 2A). The protein constructs were expressed in HEK293T cells, gently lysed in mild detergent buffer, and co-immunopurified from whole cell lysates using anti-FLAG agarose beads. The virus-host protein complexes were then reduced, alkylated, and trypsin-digested. Importantly, we used tandem mass tag (TMT)-based multiplexing using TMTpro-16plex or TMT-11plex for a relative quantification of protein abundances. For this purpose, 4−6 co-immunoprecipitation (Co-IP) replicates for the respective nsp2 homologues were pooled into a single MS run. Co-IPs from mock green fluorescent protein (GFP) transfected cells were included to differentiate the nonspecific background proteins (Figure 2B). Overall, the data set included three individual MS runs containing 34 Co-Ips (SARS-CoV-2 $n = 13$; SARS-CoV-1 $n = 9$; GFP (mock) $n = 12$) (Figure S2A).

We first determined interactors of the individual nsp2 homologues by comparing the log-transformed TMT intensity differences for prey proteins between bait and GFP samples (Figure 2C,D). We optimized variable cutoffs for high- and medium-confidence interactors based on their magnitude of enrichment compared to the GFP samples and confidence as defined by adjusted p-values (Figure 2C,D and Figure S2B,C). Using the most stringent cutoff, we identified 6 and 11 high-confidence interactors for SARS-CoV-2 and SARS-CoV-1 nsp2, respectively (Figure 2C,D). Including medium-confidence interactors, we identified 20 nsp2 interactors for each homologue, including four overlapping proteins, ERLIN1, ERLIN2, RNF170, and TMEM199 (Figure 2E).

Gene enrichment analysis shows nsp2 interactors are involved in a number of host cell processes, including metabolic processing and transport (Figure S3A). A number of these interactors are membrane-associated proteins in the ER and nucleus (Figure S3B). Detailed comparisons of gene set enrichments for individual nsp2 homologues revealed several pathways preferentially enriched for SARS-CoV-1, such as mitochondrial calcium ion transport, protein deacetylation, and negative regulation of gene expression (Figure S3C). We confirmed by immunofluorescence that SARS-CoV-1 and SARS-CoV-2 nsp2 are largely localized perinuclear and colocalize partially with the ER marker PDIA4 (Figure S3D). Nsp2 expression appears to be limited to a subset of cells as seen by immunofluorescence staining, indicating low transfection efficiency. This indicates that the identified interactions are occurring in the subset of transfected cells processed in this study. Nonetheless, the transfection efficiency was sufficient to detect nsp2 and protein interaction partners by western blot and mass spectrometry analysis.

To validate our findings, we cross referenced our data set with previous coronavirus interactomics studies. A prior study of SARS-CoV-1 nsp2 identified 11 host interactors, five of which overlap with our SARS-CoV-1 list, including GIGYF2, PHB, PHB2, STOML2, and EIF4E2.[17] We also cross referenced our interactors with a recently published SARS-CoV-2 interactomics data set.[18] Interestingly, we identified 18 new interactors, though several of these share secondary interactions with the proteins identified by Gordon et al. (Figure S4). In addition, we cross referenced our host interactor data set with tissue- and cell line-specific protein expression data sets to determine interactor expression levels in tissues associated with primary infection (Figure S5).[26−28] We find that the expression of identified interactors is enriched in lung and upper aerodigestive tissues in multiple proteomics data sets, confirming the relevance of these factors to coronavirus tropism.

Quantitative Comparison of SARS-CoV-1 and SARS-CoV-2 Interactors. Apart from determining nsp2 host cell interactors, we sought to understand to what degree interactions vary between SARS-CoV-1 and SARS-CoV-2. Our multiplexed analysis enabled direct comparison of TMT intensities between the SARS-CoV-1 and SARS-CoV-2 nsp2 Co-IPs (Figure 3A). We validated that nsp2 bait levels are largely invariable across the replicates, enabling the direct comparison of prey protein intensities (Figure S2D). We find a subset of interactors is clearly enriched for SARS-CoV-1, including GIGYF2, HDAC8, EIF4E2, and PHB2 (Figure 3A). In contrast, several other interactors are enriched more strongly for SARS-CoV-2, for instance, FOXK1 and NR2F2.

We performed unbiased hierarchical clustering of the enrichment intensities to group the nsp2 interactors in an unbiased way. This analysis yielded four distinct clusters. On the one hand, clusters 1 and 2 contained shared interactors between SARS-CoV-1 and SARS-CoV-2 nsp2. On the other hand, clusters 3 and cluster 4 contained proteins that bound exclusively to either SARS-CoV-2 or SARS-CoV-1, respectively (Figure 3B). To better visualize the relationship between the shared and unique nsp2 interactors, we constructed a network plot (Figure 3C). We also included experimentally validated secondary interactions from the STRING database to group-shared and unique interactors into functionally relevant subclusters.

Several of these subclusters are shared between SARS-CoV-1 and SARS-CoV-2 nsp2, for instance, one including STOML2, PHB, PHB2, and VDAC2. These proteins were previously shown to interact and upregulate the formation of metabolically active mitochondrial membranes.[29] Another subcluster involves ERLIN1, ERLIN2, and RNF170, which form a known complex regulating ubiquitination and degradation of inositol 1,4,5-triphosphate receptors (IP_3Rs), which in turn are channels regulating Ca^{2+} signaling from the ER to the mitochondria. Consistent with this, we detect mitochondrial calcium ion transmembrane transport as one of the unique biological processes associated with SARS-CoV-1 nsp2 but not SARS-CoV-2 (Figure S3C). Interestingly, ERLIN1 and ERLIN2 show stronger interactions with SARS-CoV-1 nsp2 than with SARS-CoV-2, indicating some strain-specific preference, which was confirmed by a western blot analysis of homologue co-IPs (Figure S6A). Additional shared interactors include a subunit of the vacuolar ATPase (ATP6AP1) (ATP = adenosine triphosphate) and a regulatory protein (TMEM199), supporting a common role for nsp2 to influence lysosomal processes. Finally, we observe one cytosolic and one ER-resident Hsp70 chaperone (HSPA8,

https://dx.doi.org/10.1021/acsinfecdis.0c00500
ACS Infect. Dis. 2020, 6, 3174−3189

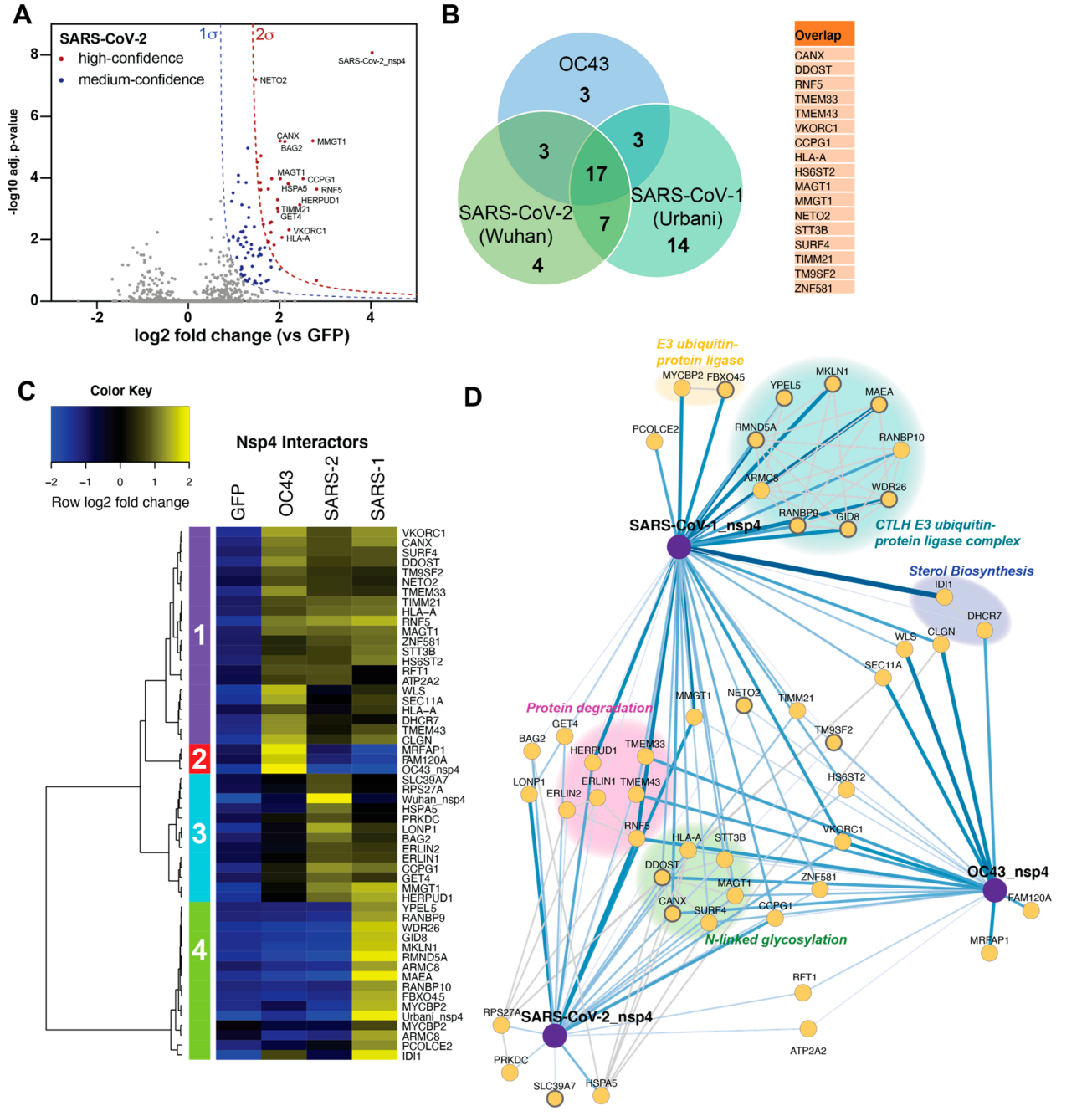

Figure 4. Comparative profiling of nsp4 interactions. (A) Volcano plot of the SARS-CoV-2 nsp4 data sets to identify medium- and high-confidence interactors. Plotted are log2 TMT intensity differences for proteins between nsp4 bait channels and GFP mock transfections vs −log10 adjusted *p*-values. Curves for the variable cutoffs used to define high-confidence (red) or medium-confidence (blue) interactors are shown. $1\sigma = 0.66$. Equivalent volcano plot for SARS-CoV-1 and OC43 nsp4 are shown in Figure S5B,C. (B) Venn diagram of interactors from nsp4 homologues. Overlapping nsp4 interactors between all strains are listed in the adjacent table. (C) Heatmap comparing the enrichment of interactors for the different nsp4 homologues. log2 fold change is color-coded and centered by row (blue low, yellow high enrichment). Hierarchical clustering using Ward's method shown on the left was performed on euclidean distances of log2 fold changes scaled by row. Cluster 1 corresponds to the shared interactors of SARS-CoV-1, -2, and OC43 nsp4. Clusters 2 and 4 contain unique interactors for OC43 and SARS-CoV-1 nsp4, respectively, while cluster 3 contains the shared interactors of SARS-CoV-1 and SARS-CoV-2. (D) Protein−Protein interaction (PPI) network map of interactors of nsp4 homologue. Blue lines indicate measured viral-host PPIs, where line width corresponds to fold enrichment compared to the GFP control. Gray lines indicate annotated host−host PPIs in STRING (score > 0.75). Groups of interactors with a common functional role are highlighted.

HSPA5) as shared interactors, highlighting their role in nsp2 folding and biogenesis.

Unique SARS-CoV-2 interactors include FOXK1 and NR2F2, both of which are antiviral transcription factors induced in response to other viruses.[30,31] We also observe an exonuclease regulator of endosomal nucleic acid sensing (PLD3),[32] a transcription factor associated with the influenza humoral response (MAZ),[33,34] and a DNA-binding protein implicated in B cell class switching (KIN or KIN17).[35] In contrast, the list of unique SARS-CoV-1 interactors includes components of the 4EFP-GYF2 translation repression complex (GIGYF2, EIF4E2), lysosomal ion channels involved in

https://dx.doi.org/10.1021/acsinfecdis.0c00500
ACS Infect. Dis. 2020, 6, 3174−3189

chloride/proton ion exchange (CLCN7, OSTM1), and the cytosolic histone deacetylase 6 (HDAC6). While SARS-CoV-1 interactors GIGYF2 and EIF4E2 were also identified in the recent SARS-CoV-2 nsp2 data set,[18] it is clear from our quantitative comparison that enrichment of this complex with SARS-CoV-2 nsp2 is much weaker than with SARS-CoV-1 nsp2.

Comparative Profiling of CoV nsp4 Interactions. We extended our comparative analysis of host cell interactors to another CoV nonstructural protein, nsp4, involved in the replication complex. We applied the same AP-MS workflow used to identify nsp2 interactors (Figure 2A). In addition to SARS-CoV-1 and SARS-CoV-2 nsp4, we also included the hCoV-OC43 nsp4 construct. With this addition, we sought to probe the protein−protein interactions that differentiate strains causing severe pathogenesis versus nonsevere. To this end, four co-immunoprecipitation replicates of the respective nsp4 homologues were pooled into a single MS run, along with mock GFP-transfected cells to differentiate nonspecific background proteins (Figure 2B). The full data set included three individual MS runs, containing 40 Co-IPs (SARS-CoV-2 n = 12; SARS-CoV-1 n = 8; OC43 n = 8; GFP (mock) n = 12) (Figure S7A).

As previously described, we optimized variable cutoffs for high- and medium-confidence interactors based on their magnitude enrichment compared to GFP samples (Figures 4A and S7B,C). We identified 29, 20, and 13 high-confidence interactors for SARS-CoV-2, SARS-CoV-1, and OC43, respectively, using the most stringent cutoff (Figures 4A and S7B,C). Including medium-confidence interactors, we identified 86, 126, and 93 nsp4 interactors for SARS-CoV-2, SARS-CoV-1, and OC43 nsp4 homologues, respectively. Comparisons of high-confidence interactors yielded 17 shared interactors between all strains (Figure 4B) or 30 medium-confidence shared interactions (Figure S7D).

Similarly to our analysis of nsp2, we compared our data set with previously published nsp4 interactomics data, including the recently published study of the SARS-CoV-2 interactome,[18] and found there is relatively little overlap between our identified SARS-CoV-2 nsp4 interactors and the published nsp4 interactomics data (Figure S8). This discrepancy could be attributed to the nsp4 constructs in our study including the C-terminal residues of nsp3, which were added to ensure proper localization and prevent the hydrophobic N-terminal region of nsp4 to serve as a signal sequence.[24] For further validation, we determined interactor expression levels in human tissues and found interactors are enriched in tissues relevant to coronavirus tropism (Figure S5).[26−28]

Analysis of the gene ontology (GO) terms associated with the nsp4 interactors showed multiple enriched biological processes, such as cell organization and biogenesis, transport, and metabolic processes (Figure S9A). Interestingly, several shared SARS nsp4 interactors are associated with cell death, cellular communication, and cell differentiation. The shared interactors of all three strains are predominantly ER-membrane-associated proteins, while many SARS-CoV-1 and OC43 specific interactors are annotated as nuclear localized (Figure S9B). Comparisons of gene-set enrichment analysis between strains indicate the ER-associated degradation (ERAD) pathway is significantly enriched for SARS strains, most strongly for SARS-CoV-1 (Figure S9C). Ubiquitin-dependent protein catabolic processes and ER mannose trimming are also strongly enriched for SARS-CoV-1. In general, processes strongly enriched for SARS-CoV-1 are less enriched for SARS-CoV-2 and to an even lesser extend for OC43.

Our multiplexed analysis of the nsp4 homologue Co-IPs enabled direct comparison across strains (Figure S10A−C). We validated that nsp4 bait levels were mostly similar across replicates, allowing for a direct comparison of the bait protein intensities (Figure S10D). The unbiased hierarchical clustering of enrichment intensities to group nsp4 interactors yielded four distinct clusters. Cluster 1 contained common interactors of all nsp4 homologues (Figure 4C), while cluster 3 contained shared interactors of SARS-CoV-2 and SARS-CoV-1 nsp4 that displayed weaker enrichment with OC43. In contrast, clusters 2 and 4 contained unique interactors enriched for OC43 and SARS-CoV-1 nsp4, respectively. To visualize functionally relevant subclusters of shared and unique nsp4 interactors, we constructed a network plot, including high-confidence interactions (score > 0.75) from the String database (Figure 4D). Inclusion of all median-confidence interactors of the nsp4 homologues yielded a similar clustering and network organization (Figures S10E and S11).

We identified several common interactors across all three nsp4 homologues. These include components of the UPR signaling (TMEM33) and ER-phagy (CCPG1). We also identify RNF5, an ER-localized E3 ubiquitin ligase known to modulate antiviral innate immune signaling,[36,37] and VKORC1, which reduces Vitamin K, a key cofactor for several coagulation factor proteins.[38] Not surprisingly, given that nsp4 is a glycosylated protein, we also identify several members of the N-linked glycosylation machinery (STT3B, MAGT1, CANX, DDOST) (Figure 4D) in all three strains.

We identified several shared interactors between SARS-CoV-1 and SARS-CoV-2 that were absent in OC43. These include the ERLIN1/2 complex, LONP1, HERPUD1, GET4, and BAG2, all of which are involved in a facet of ER homeostasis, proteostasis, or trafficking (Figure 4D). We validated the interactions of nsp4 constructs with ERLIN2 and CANX by Co-IP and confirmed that ERLIN2 enriches significantly more strongly with SARS-CoV-1 and -2 compared to OC43, while CANX interacts with all three homologues (Figure S6A). The ERLIN1/2 complex was also identified in the nsp2 data set (Figure 3B,C) and shows comparable enrichment values between SARS-CoV-1 and SARS-CoV-2. Interestingly, the other four overlapping interactors all exhibit increased enrichment for SARS-CoV-2 versus SARS-CoV-1. LONP1 is a mitochondrial peptidase responsible for removing the majority of damaged mitochondrial proteins via proteolysis. The UPR induces HERPUD1 expression, which is involved in the ERAD pathway to maintain ER homeostasis.[39] BAG2 serves as a cochaperone for HSP70 chaperones, acting as a nucleotide exchange factor to regulate chaperone-client interactions through modulating HSP70 ATPase rates,[40] while GET4 is part of a complex driving trafficking of tail-anchored proteins to the ER.[41]

We observed shared interactors between OC43 and SARS-CoV-2, such as the N-glycosylation factor RFT1[42,43] and a sarcoplasmic/endoplasmic reticulum calcium ATPase (SERCA−ATP2A2).[44] In addition, we identified shared interactors between OC43 and SARS-CoV-1, including a regulator of UPR-mediated apoptosis (WLS or GPR177),[45] a member of the signal peptidase complex (SEC11A),[46] and factors involved in cholesterol synthesis (IDI1, DHCR7).[47−50] WLS, SEC11A, and DHRC7 exhibited a higher enrichment for

https://dx.doi.org/10.1021/acsinfecdis.0c00500
ACS Infect. Dis. 2020, 6, 3174−3189

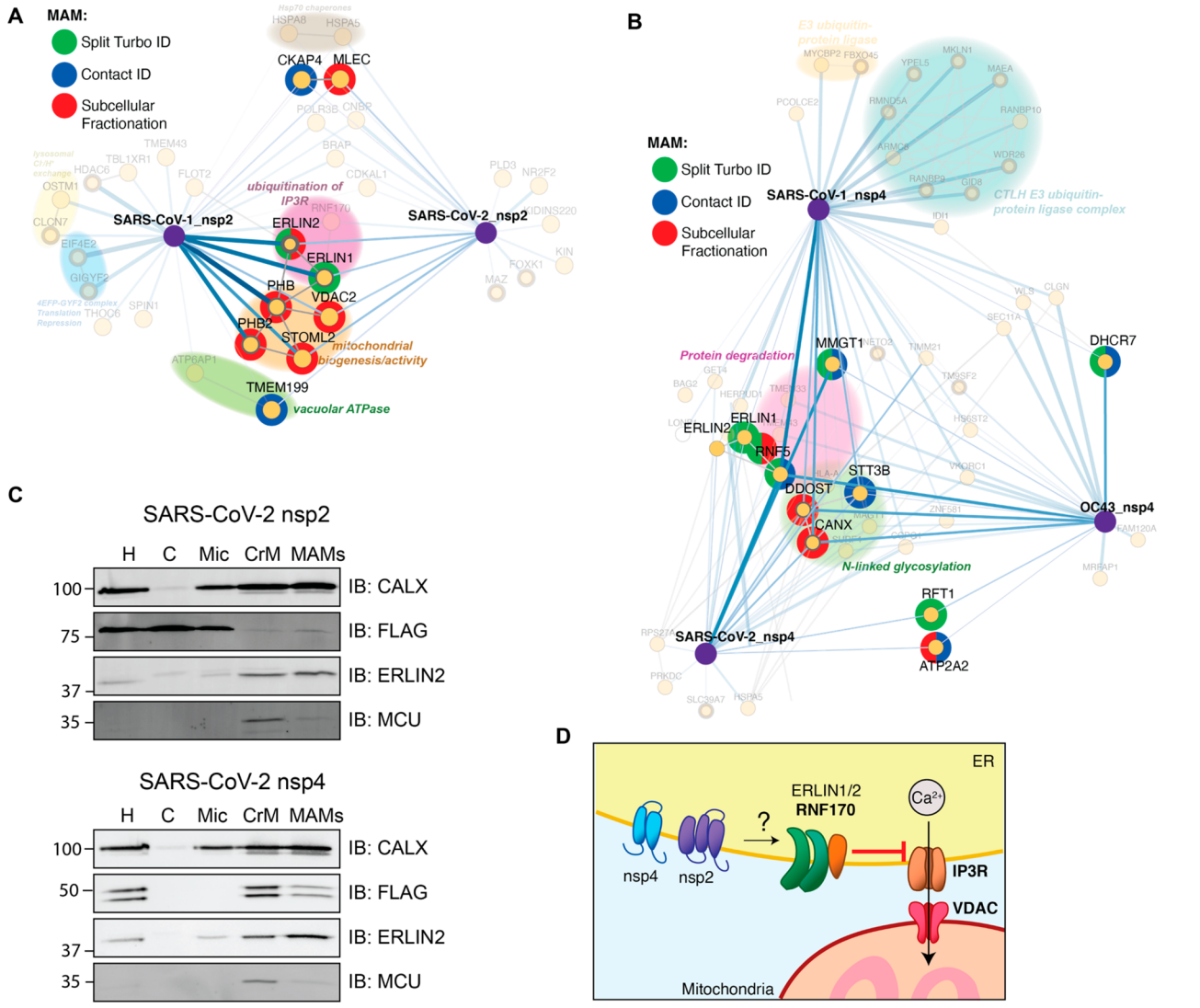

Figure 5. Enrichment of MAM proteins as nsp2 and nsp4 interactors. (A, B) Interactors of nsp2 (A) and nsp4 (B) homologue annotated for MAM proteins. The lists of interactors was cross referenced with previous publications profiling the MAM proteome (Split-Turbo ID,[55] Contact-ID,[56] and subcellular fractionation[57]). (C) Subcellular fractions of SARS-CoV-2 nsp2 or nsp4 transfected HEK293T cells to determine the localization of viral proteins to MAMs. Homogenate (H), cytosol (C), microsome (Mic), crude mitochondria (CrM), and MAMs fractions were probed via western blot for subcellular markers (CALX and ERLIN2 for MAMs; MCU for mitochondria) and viral proteins (FLAG). Subcellular fractionation was performed in triplicate, and representative blots are shown. (D) Proposed model for how SARS-CoV nsp2 and nsp4 utilize ERLIN1/2 and interacting protein factors to regulate ER Ca^{2+} signaling at MAMs.

OC43, whereas IDI1 was more greatly enriched for SARS-CoV-1. Consistent with this observation, we identified the sterol metabolic process as one of the unique processes enriched for OC43 nsp4.

In addition to shared interactors, we found several unique interactors for SARS-CoV-2, including the monoubiquitin-ribosomal fusion protein (RPS27A), a Golgi/ER-resident zinc receptor that has been shown to regulate tumor necrosis factor (TNF) receptor trafficking and necroptosis (SLC39A7), and the ER-resident Hsp70 chaperone BiP (HSPA5). The latter two play distinct roles in regulating ER homeostasis and proteostasis. In contrast, only two unique OC43 nsp4 interactors were identified: a target of the NEDD8-Cullin E3 ligase pathway (MRFAP1)[51] and FAM120A, an RNA-binding protein found to serve as a scaffolding protein for the IL13 signaling pathway (Figure S10B,C).[52,53] Both of these proteins are localized to the nucleus (Figure S9B). Lastly, we identified a large cluster of unique SARS-CoV-1 nsp4 interactors that compose the CTLH E3 ubiquitin ligase complex (Figure 4D). This nuclear complex maintains cell proliferation rates, likely through the ubiquitination of the transcription factor Hbp1, a negative regulator of cell proliferation.[54] This complex is highly enriched for SARS-CoV-1 specifically, presenting one of the most profound differences in interaction profile (Figure S8A,C). This specificity of engagement was validated through Co-IP and western blot (Figure S6A,B). We confirmed that only SARS-CoV-1 nsp4 copurified with several components of the CTLH complex (MKLN1, WDR26, RANBP9).

The fact that both OC43 and SARS-CoV-1 nsp4 displayed prominent interactions with nuclear proteins prompted us to evaluate the cellular localization of the protein by immunofluorescence. We detected perinuclear puncti for all constructs that partially colocalized with the ER marker PDIA4 (Figure S12), consistent with prior studies.[22] However, for SARS-CoV-1 and OC43 nsp4, we also detected a measurable signal in the nucleus, supporting a nuclear function and the observed

https://dx.doi.org/10.1021/acsinfecdis.0c00500
ACS Infect. Dis. 2020, 6, 3174−3189

interactions with proteins in the nucleus. As observed with the nsp2 expression, immunofluorescence staining indicated that nsp4 expression was limited to a low number of cells within the transfected plates, implying that identified interactions originate from a subset of cells.

Enrichment of Mitochondria-Associated Membrane Proteins as nsp2 and nsp4 Interactors. In our evaluation of cellular compartment GO terms, we noticed that nsp2 and nsp4 interactors are enriched in membranes of the endoplasmic reticulum and the mitochondria (Figures S3B and S9B). In particular, ERLIN1/2 and RNF170 form an E3 ubiquitin ligase complex known to localize to the interface between the ER and mitochondria, regions termed mitochondria-associated membranes (MAMs). We therefore probed our data set for any other MAMs-associated nsp2 and nsp4 interactors. We cross-referenced our interactor lists with three published data sets that specifically characterized the MAMs proteome[55−57] and identified 17 proteins associated with MAMs (Figure 5A,B). Seven of these factors solely interact with nsp2, eight proteins solely interact with one or more strains of nsp4, and the ERLIN1/2 complex interacts with both nsp2 and nsp4 (Figures 3C and 4D). Interestingly, the ERLIN1/2 complex only interacts with SARS-CoV-1 and -2 proteins and not OC43. SARS-CoVs may use ERLIN1/2 to regulate ER Ca^{2+} signaling and the myriad of downstream host processes controlled by this signaling pathway (Figure 5D).

To determine if nsp2 or nsp4 indeed colocalize to MAMs, we performed subcellular fractionation and probed for the presence of viral proteins in MAMs fractions, as well as various fraction markers (CALX and ERLIN2 for MAMs, MCU for mitochondria) by western blotting (Figure 5C and Figure S13). We find that both SARS-CoV-2 nsp2 and nsp4 are detected in MAMs, though nsp4 is more enriched at MAMs than nsp2 (Figure 5C). SARS-CoV-1 nsp2 is absent from the MAMs fractions, while both SARS-CoV-1 and hCoV-OC43 nsp4 are strongly enriched in MAMs (Figure S13).

DISCUSSION

Our analysis enables both the identification of interactors for SARS-CoV-1, SARS-CoV-2, and OC43 homologues of nsp2 and nsp4 and a comparative quantitative enrichment to differentiate between shared and unique host cell binding partners. We acknowledge the limitations of using transiently transfected viral proteins for AP-MS. Viral infection is a collection of both protein−protein and RNA−protein interactions, and our approach of single protein expression may omit direct interactions that would result from the full context of virus replication. In addition, transient and low-affinity interactions may not be identified using our current approach. Additional incorporation of chemical cross-linkers may be necessary to capture such transient interactors. However, given the logistical barriers to handling BSL-3 viruses, paired with the urgency of the current pandemic, our workflow is an efficient system to perform comparative analysis and generate a shortlist of interactors to prioritize for further investigation. Furthermore, some direct interactions of CoV proteins may be short in duration and missed by interaction mapping in full virus infection. Thus, relevant but short-lived interactions may be better identified through individual protein expression.

We identify several nsp2 interactors shared across SARS strains, including STOML2, and prohibitins (PHB and PHB2), which were previously identified as interacting with SARS-CoV-1.[17] These proteins work in tandem to induce the formation of metabolically active mitochondrial membranes to regulate mitochondrial biogenesis. Increased levels of STOML2 are associated with increased ATP production and reduced apoptosis induction.[29] This conserved interaction for SARS strains presents an avenue for nsp2 to increase mitochondrial metabolism and stall apoptosis to maintain a pro-viral cellular environment. Additionally, STOML2 has been found to play a key role in stabilizing hepatitis C virus replication complexes,[58] and PHB has been shown to promote entry of both Chikungunya virus[59] and enterovirus 71.[60] These factors may prove effective pan-RNA virus targets for host-directed therapies. We also attempted to extend the comparative analysis to OC43 nsp2. However, this construct did not express detectable protein, which could be due to a much lower homology to SARS-CoV-2 and SARS-CoV-1 than for other nonstructural proteins.

For nsp4, we identify multiple unique SARS-CoV-1 interactors, most notably, members of the CTLH E3 ubiquitin ligase complex. This complex is known to regulate levels of Hbp1, a negative regulator of proliferative genes,[54] and was previously shown to interact with the dengue virus NS2B/NS3 proteins,[15] implicating this complex as a target for RNA viruses to influence cell proliferation. We also identified the FBXO45-MYCBP2 E3 ubiquitin ligase complex, which has been shown to prevent cell death in mitosis.[61] Together, this may support a role in SARS-CoV-1 nsp4 co-opting host ubiquitin complexes to extend cell viability during infection to promote viral replication. During resubmission, Gordon et al. published a comparative coronavirus interaction network confirming the SARS-CoV-1 specific interactions with the CTLH E3 ligase complex.[62]

Furthermore, we find components of the cholesterol biosynthesis pathway, IDI1 and DHCR7, which were specifically enriched for SARS-CoV-1 and OC43 nsp4, respectively. IDI1 has been shown to be downregulated by host cells in response to cytomegalovirus (CMV)-infection-induced interferons[47] and is upregulated by both human immunodeficiency virus (HIV) and hepatitis C virus (HCV) during infection.[48,49] DHCR7 is downregulated during RNA virus infection in macrophages to promote IRF3 signaling and IFN-1 production. Moreover, the inhibition of DHCR7 aids in the clearance of multiple RNA viruses.[50] These previous findings indicate that interactions with IDI1 and DHCR7 may provide a means for coronaviruses to counteract antiviral responses. Interestingly, these interactions with the aforementioned E3 ligase complexes and cholesterol biogenesis factors are not enriched for SARS-CoV-2 nsp4, implying that SARS-CoV-2 pathogenesis may not require these interactions.

As a whole, it appears that SARS-CoV-2 homologues differ from SARS-CoV-1 not by gaining new interactions but rather by losing network nodes. This is emphasized in the gene enrichment analysis of nsp2 and nsp4 (Figures S3C and S9C), in which multiple pathways are more strongly enriched for SARS-CoV-1, as well as in the nsp4 interactome (Figure 4C,D), particularly with the absence of E3 ligase complex interactions for SARS-CoV-2. It will be important to investigate potential functional implications of the engagement of these E3 ubiquitin ligases, as well innate immune signaling factors, on CoV infections and the course of pathogenicity for the divergent strains.

To gain functional insights into which nsp2 and nsp4 interactions may have an impact on CoV infection, we mined

https://dx.doi.org/10.1021/acsinfecdis.0c00500
ACS Infect. Dis. 2020, 6, 3174−3189

recently published data from a genome-wide clustered regularly interspaced short palindromic repeats (CRISPR) knockout screen and a targeted siRNA knockdown/CRISPR knockout screen of SARS-CoV-2 interactors (Figure S14A,B).[62,63] The comprehensive genome-wide data set by Heaton et al. conducted in A549 lung cancer cells identified that knockout of several of the proteostasis components (BAG2, DDOST), as well as ERLIN1 and ERLIN2 enhanced cell survival in the presence of SARS-CoV-2, suggesting that these factors may have an antiviral function (Figure S14A). When comparing the more limited siRNA knockdown data in A549 cells and CRISPR knockout data in Caco2 colorectal cancer cells, ATP6AP1 stood out as hampering SARS-CoV-2 infection in both cell models supporting a pro-viral role (Figure S14B).[62] ATP6AP1/Ac45 is a critical accessory subunit to facilitate the assembly of the vacuolar ATPase in support of lysosome function and autophagy playing a role in viral infection.[64] Future functional genomic screens will be necessary to evaluate the role of other interactors on CoV infection and evaluate differential roles for the distinct strains.

A particularly noteworthy finding is the identification of 17 MAMs factors in the combined nsp2 and nsp4 data sets, based on cross-referencing interactors with previously published proteomics studies of MAMs proteins.[55−57] Given the prominence of these interactions, it is tempting to speculate that nsp2 and nsp4 localize to MAMs and influence processes at these important organelle contact sites (Figure 5D). MAMs are nodes for innate immune signaling and apoptosis pathways, both of which are common targets for viral manipulation.

In particular, we identify the E3 ubiquitin ligase RNF5 interacting with all nsp4 homologues. RNF5 targets STING for degradation, which stabilizes retinoic acid-inducible gene-I (RIG-I) and mitochondrial antiviral-signaling protein (MAVS) interactions at MAMs, thereby inducing interferon-1 and -3 production via IRF3 and NF-κB signaling.[36,37] RIG-I is one of the main viral RNA genome sensors in host cells; therefore, it is possible that nsp4 increases the targeting of RNF5 to MAMs to inhibit the downstream signaling of RIG-1.

We also identify the ERLIN1/2 complex in both nsp2 and nsp4 data sets. In the nsp2 interaction network, the complex is associated with a different E3 ligase, RNF170. RNF170 has been shown to inhibit innate immune signaling by targeting TLR3 for degradation, thereby blocking IRF3 and NF-κB signaling pathways.[65] In addition, ERLIN1/2 acts in concert with RNF170 to target the inositol-1,4,5-triphophate receptor (IP_3R) for degradation via polyubiquination.[66] IP_3R is an ER-resident Ca^{2+} channel integral in the formation of MAMs.[67,68] Calcium flux at the MAMs has been shown to increase mitochondrial calcium uptake, which increases ATP production, thereby benefiting active viral replication.[69] Indeed, several other viruses have been shown to influence ER Ca^{2+} exchange. For instance, the Hepatitis C viral protein, NS5A, promotes the degradation of IP_3R3 to limit apoptosis induction triggered by persistent Ca^{2+} signaling at MAMs.[70] Previous studies have shown the SARS-CoV-1 E protein acts as a channel to leak ER calcium stores during infection,[71] but to our knowledge, no such features have been attributed to either nsp2 or nsp4. Thus, manipulation of ER Ca^{2+} signaling via IP_3R regulation may represent a novel method by which coronaviruses manipulate mitochondrial function (Figure 5D). In support of this, we find that both SARS-CoV-2 nsp2 and nsp4 colocalize to MAMs using subcellular fractionation (Figure 5C). Additionally, a recent study found that IP_3R3 is significantly upregulated during SARS-CoV-2 infection[72] (Figure S14C). Further studies will be important to evaluate whether ER calcium exchange and mitochondrial metabolism could impact coronavirus infection.

METHODS

Protein Expression Constructs. Coding sequences for nsp2 and nsp4 were obtained from GenBank (MN908947 SARS-CoV-2 isolate Wuhan-Hu-1; AY278741 SARS-CoV-1 Urbani; NC_006213 hCoV OC43 strain ATCC VR-759). Human codon optimized sequences were designed, and genes were synthesized and cloned into pcDNA3.1-(+)-C-DYK (nsp4) to append a C-terminal FLAG tag or into pcDNA3.1-(+)-N-DYK (nsp2) to append an N-terminal FLAG tag (GenScript).

Cell Culture and Transfection. HEK293T cells were maintained in Dulbecco's Modified Eagle's Medium (DMEM) with high glucose and supplemented with 10% fetal bovine serum (FBS), 1% penicillin/streptomycin, and 1% glutamine. Cells were kept at 37 °C, 5% CO_2. Generally, 2×10^6 cells were seeded into 10 cm dishes. At 24 h postseeding, the cells were transfected with 5 μg of nsp2, nsp4, or fluorescent control DNA constructs in pcDNA3.1-(+)-C/N-DYK vectors using a calcium phosphate method. Media was exchanged 16 h post-transfection, and the cells were harvested 24 h after the media were changed.

Immunoprecipitation. Cells were collected and washed with phosphate-buffered solution (PBS). Immunoprecipitation samples were lysed by resuspension in TNI buffer (50 mM Tris pH 7.5, 150 mM NaCl, 0.5% IGEPAL-CA-630) with Roche cOmplete protease inhibitor on ice for at least 10 min, followed by sonication in a room-temperature water bath for 10 min. Lysates were cleared by centrifugation at 17 000*g* for 10−20 min. Sepharose 4B resin (Sigma) and G1 anti-DYKDDDDK resin (GenScript) were prewashed four times with the respective lysis buffer for each sample. Protein concentrations in cleared lysates were normalized using BioRad Protein Assay Dye and added to 15 μL of Sepharose 4B resin for 1 h, rocking at 4 °C. Resin was collected by centrifugation for 5−10 min at 400*g*, and precleared supernatant was added directly to 15 μL of G1 anti-DYKDDDDK resin and rocked at 4 °C overnight. The next day, the supernatant was removed, and the resin was washed four times with the respective lysis buffer. Bound proteins were eluted with the addition of modified 3X Laemelli buffer (62.5 mM Tris, 6% sodium dodecyl sulfate (SDS)) for 30 min at room temperature followed by 15 min at 37 °C, followed by a second elution for 5−15 min at 37 °C. 10% of the elution was set aside for SDS poly(acrylamide) gel electrophoresis (PAGE) and silver staining to confirm immunoprecipitation efficiency, and the remainder was prepared for mass spectrometry. Silver staining was performed using a Pierce Silver Stain kit (Thermo Scientific). Separate biological replicates of co-immunoprecipitated lysates were identically processed, in which inputs and elutions were normalized and run on SDS-PAGE gel, transferred to poly(vinylidene fluoride) (PVDF) membrane, and blotted for various host interactors using the following antibodies (1:1000 dilutions): anti-FLAG (Sigma-Aldrich, F1804), anticalnexin (GeneTex, GTX109669), antimuskelin (Santa Cruz Biotechnology, SC-398956), anti-ERLIN2 (Sigma-Aldrich, HPA002025), and anti-GAPDH (GeneTex, GTX627408) as a loading control.

https://dx.doi.org/10.1021/acsinfecdis.0c00500
ACS Infect. Dis. 2020, 6, 3174−3189

Tandem Mass Tag Sample Preparation. The sample preparation was performed as described.[73] Briefly, the eluted proteins were precipitated in methanol/chloroform/water (3:1:3) and washed twice in methanol, and the protein pellets were air-dried. The pellets were resuspended in 1% Rapigest SF (Waters), reduced, and alkylated. The proteins were digested in trypsin-LysC overnight. The digested peptides were labeled using 11-plex or 16-plex tandem mass tag (TMT or TMTpro) reagents (Thermo Scientific), pooled, and acidified using formic acid. Cleaved Rapigest was removed by centrifugation of samples at 17 000*g* for 30 min.

MudPIT Liquid Chromatography−Mass Spectrometry Analysis. Triphasic MudPIT microcolumns were prepared as described.[74] Individual pooled TMT proteomics samples were directly loaded onto the microcolumns using a high-pressure chamber followed by a wash with 5% acetonitrile and 0.1% formic acid in water (v/v) for 30 min. The peptides were analyzed by liquid chromatography−mass spectrometry on an Exploris 480 in line with an Ultimate 3000 nanoLC system (Thermo Fisher). The MudPIT microcolumns were installed on a column-switching valve on the nanoLC systems followed by 20 cm fused silica microcapillary column (ID 100 μm) ending in a laser-pulled tip filled with Aqua C18, 3 μm, 100 Å resin (Phenomenex). MudPIT runs were performed by a 10 μL sequential injection of 0, 10, 20, 40, 60, 80, 100% buffer C (500 mM ammonium acetate, 94.9% water, 5% acetonitrile, 0.1% formic acid), followed by a final injection of 90% C, 10% buffer B (99.9% acetonitrile, 0.1% formic acid v/v). Each injection was followed by a 130 min gradient using a flow rate of 500 nL/min (0−6 min: 2% buffer B, 8 min: 5% B, 100 min: 35% B, 105 min: 65% B, 106−113 min: 85% B, 113−130 min: 2% B). Electrospray ionization was performed directly from the tip of the microcapillary column using a spray voltage of 2.2 kV, ion transfer tube temperature of 275 °C, and radio frequency (RF) lens of 40%. MS1 spectra were collected using the following settings: scan range of 400−1600 m/z, 120 000 resolution, automatic gain control (AGC) target 300%, and automatic injection times. Data-dependent tandem mass spectra were obtained using the following settings: monoisotopic peak selection mode: peptide, included charge state 2−7, TopSpeed method (3 s cycle time), isolation window 0.4 m/z, higher-energy collisional dissociation (HCD) fragmentation using a normalized collision energy of 32 for TMTpro and 36 for TMT, resolution 45 000, AGC target 200%, automatic injection times, and dynamic exclusion (20 ppm window) set to 60 s.

Experimental Layout and Data Analysis. The nsp2 AP-MS experiments included three individual MS runs combining 34 Co-AP samples (SARS-CoV-2 n = 13; SARS-CoV-1 n = 9; GFP (mock) n = 12). The samples were distributed to TMTpro 16plex or TMT11plex channels as outlined in Figure S2A. The nsp4 AP-MS experiments consisted of three individual MS runs, containing 40 Co-IPs (SARS-CoV-2 n = 12; SARS-CoV-1 n = 8; OC43 = 8; GFP (mock) n = 12). The samples were distributed to TMTpro 16plex channels as outlined in Figure S5A. The identification and quantification of peptides and proteins were performed in Proteome Discoverer 2.4 (Thermo Fisher) using a SwissProt human database (Tax ID 9606, release date 2019-11-23). CoV nsp2 and nsp4 protein sequences were added manually. Searches were conducted in Sequest HT using the following setting: Trypsin cleavage with max. Two missed cleavage sites, minimum peptide length 6, precursor mass tolerance 20 ppm, fragment mass tolerance 0.02 Da, dynamic modifications: Met oxidation (+15.995 Da), Protein N-terminal Met loss (−131.040 Da), Protein N-terminal acetylation (+42.011 Da), static modifications: Cys carbamidomethylation (+57.021 Da), TMTpro or TMT6plex at Lys and N-termini (+304.207 Da for TMTpro or +229.163 for TMT6plex). Peptide IDs were filtered using the Percolator node using an false discovery rate (FDR) target of 0.01. Proteins were filtered based on a 0.01 FDR requiring two peptide IDs per protein, and protein groups were created according to a strict parsimony principle. TMT reporter ions were quantified using the reporter ion quantification considering unique and razor peptides and excluding peptides with coisolation interference greater than 25%. Peptide abundances were normalized based on total peptide amounts in each channel assuming similar levels of background signal in the APs. Protein quantification roll-up used all quantified peptides. The pairwise ratios between conditions were calculated based on the total protein abundances, and ANOVA on individual proteins was used to test for changes in abundances and to report adjusted p-values.

To filter high-confidence interactors of individual CoV nsp proteins, we used a variable filter combining log2 fold enrichment and adjusted p-value according to a published method.[75] Briefly, the histogram of log2 protein abundance fold changes between nsp-transfected versus mock-transfected groups were fitted to a Gaussian curve using a nonlinear least-square fit to determine the standard deviation σ (see Figure S2B,C). Fold change cutoffs for high-confidence and medium-confidence interactors were based on 2 σ or 1 σ, respectively. For actual cutoffs taking into consideration adjusted p-values, we utilized a hyperbolic curve $y > c/(x - x_0)$, where y is the adjusted p-value, x is the log2 fold change, x_0 corresponds to the standard deviation cutoff (2 σ or 1 σ), and c is the curvature (c = 0.4 for 1 σ and 0.8 for 2 σ) (see Figures 2C,D, 4A, and S7B,C).

The mass spectrometry proteomics data were deposited to the ProteomeXchange Consortium via the PRIDE[76] partner repository with the data set identifier PXD022017.

Gene-Set Enrichment Analysis. The GO-term categories for biological processes and cellular components for interactors were based on assignment in the Proteome Discoverer Protein Annotation node. A gene-set enrichment analysis was conducted in EnrichR.[77] The analysis was conducted separately for sets of interactors of individual nsp2 or nsp4 homologues, and the GO-terms for biological processes were filtered by adjusted p-values < 0.1. Redundant GO terms were grouped manually based on overlapping genes in related terms.

Network Plots and Identification of Overlapping Interactions with Published Data. Extended and overlapping interactomes between the novel interactors identified in this study and previously published interactors[18] were generated by scraping the top n interactors of each primary prey protein on the STRING database using the python API. We established an extended secondary interactome by searching for the top 20 and top 30 STRING db interactors of the nsp4 primary interactors and nsp2 interactors, respectively, using the limit parameter in STRING API and searching against the human proteome (species 9606). We then compared the extended interactomes of our data with the previously published data by dropping any secondary interactors that did not appear in both data sets. Next, we concatenated the primary interactors from our data, the primary interactors from the published data, and the

https://dx.doi.org/10.1021/acsinfecdis.0c00500
ACS Infect. Dis. 2020, 6, 3174−3189

overlapping secondary interactors into a single data frame. Finally, we searched the overlapping secondary interactors against the STRING database human proteome to determine interactors between secondary interactors with a threshold of greater than 50% likelihood in the experimental score category. The results were plotted in Cytoscape.

Immunofluorescence Confocal Microscopy. HEK293T cells were cultured on glass-bottom culture dishes (MatTek, P35G-0-14-C) and transfected with CoV expression constructs as previously described. Cells were fixed with 4% paraformaldehyde-PBS, washed thrice with PBS, then permeabilized in 0.2% Triton-X (in PBS). After three PBS washes, the cells were blocked in PBS with 1% bovine serum albumin (BSA) with 0.1% Saponin (blocking buffer). After the blocking, the cells were incubated with anti-PDIA4 primary antibody (Protein Tech, 14712−1-AP) in blocking buffer (1:1000 dilution) for 1 h at 37 °C. After three PBS washes, the cells were incubated with Alexa Fluor 488-conjugated antirabbit goat antibody (ThermoFisher, A-11008) in a blocking buffer (1:500 dilution) at room temperature for 30 min. Cells were then stained with M2 FLAG primary antibody (SigmaAldrich, F1804) and Alexa Fluor 594-conjugated antimouse goat antibody (ThermoFisher, A-11005) using the same conditions. Cells were then mounted in Prolong Gold with 4′,6-diamidino-2-phenylindole (DAPI) stain (ThermoFisher, P36935). The cells were imaged using an LSM-880 confocal microscope (Zeiss), and the images were merged using ImageJ software.

Subcellular Fractionation. HEK293T cells were transfected with tdTomato, nsp2, or nsp4 constructs as previously described and harvested via scraping ($(1.5-2.0) \times 10^8$ cells per sample). The cells were fractionated based on a previously published protocol.[78] In brief, the cells were mechanically lysed in 6 mL of sucrose homogenization medium (250 mM sucrose, 10 mM 4-(2-hydroxyethyl)-1-piperazineethanesulfonic acid (HEPES), pH 7.4) using a douncer homogenizer (Kimbell, DD9063). Homogenate was spun four times (5 min, 600*g*, 4 °C) to pellet the cell debris and intact cells. The supernatant was then centrifuged for 10 min at 10 300*g*, 4 °C in a fixed-angle rotor to pellet the crude mitochondria. The resulting supernatant was centrifuged at 10 300*g* for 10 min at 4 °C twice more to pellet the residual crude mitochondria and then ultracentrifuged at 100 000*g* for 60 min at 4 °C to separate the microsome fraction (pellet) from the cytosolic fraction (supernatant). The crude mitochondrial pellet was resuspended in 0.5 mL of mannitol buffer A (250 mM mannitol, 0.5 mM ethylene glycol-bis(*β*-aminoethyl ether)-*N*,*N*,*N*′,*N*′-tetraacetic acid (EGTA), 5 mM HEPES, pH 7.4), layered on top of 8 mL of 30% (w/v) Percoll solution (Sigma, P1644), and then ultracentrifuged at 95 000*g* for 65 min at 4 °C to separate MAMs from the crude mitochondria. The MAMs were pelleted by centrifugation at 100 000*g* for 1 h at 4 °C. Fractions were run on SDS-PAGE gel, and the proteins detected via western blotting with the following antibodies: anti-calnexin (GeneTex, GTX109669), anti-MCU (ThermoFisher, MA5−24702), anti-FLAG (Sigma-Aldrich, F1804), and anti-ERLIN2 (Sigma-Aldrich, HPA002025).

■ ASSOCIATED CONTENT

Supporting Information

The Supporting Information is available free of charge at https://pubs.acs.org/doi/10.1021/acsinfecdis.0c00500.

Amino acid sequence comparisons and MS sequence coverage of CoV nonstructural proteins; TMT normalization and filtering of nsp2 interactors; gene ontology pathway analysis and IF localization of nsp2 homologues; nsp2 interactome overlap with published data set; tissue-specific expression of nsp2 and nsp4 interactors; coimmunoprecipitation western blots of MAMs factors with CoV nonstructural proteins; TMT normalization and filtering of nsp4 interactors; nsp4 interactome overlap with published data set; gene ontology pathway analysis of nsp4 interactors (PDF)

Comparative analysis of nsp4 homologues (PDF)

Network map of high- and medium-confidence nsp4 homologue interactors (PDF)

IF subcellular localization of nsp4 homologues (PDF)

Localization of SARS-CoV_1 nsp2, nsp4, and OC43 nsp4 to MAMs (PDF)

Mining of published functional genomic screens of interactors in SARS-CoV-2 infection (PDF)

Tables listing relevant proteomics data and information (PDF)

■ AUTHOR INFORMATION

Corresponding Author

Lars Plate − *Department of Biological Sciences and Department of Chemistry, Vanderbilt University, Nashville, Tennessee, United States; Vanderbilt Institute for Infection, Immunology and Inflammation, Vanderbilt University Medical Center, Nashville, Tennessee, United States;* orcid.org/0000-0003-4363-6116; Phone: (615)-343-3405; Email: lars.plate@vanderbilt.edu

Authors

Jonathan P. Davies − *Department of Biological Sciences, Vanderbilt University, Nashville, Tennessee, United States; Vanderbilt Institute for Infection, Immunology and Inflammation, Vanderbilt University Medical Center, Nashville, Tennessee, United States*

Katherine M. Almasy − *Department of Chemistry, Vanderbilt University, Nashville, Tennessee, United States; Vanderbilt Institute for Infection, Immunology and Inflammation, Vanderbilt University Medical Center, Nashville, Tennessee, United States*

Eli F. McDonald − *Department of Chemistry, Vanderbilt University, Nashville, Tennessee, United States; Vanderbilt Institute for Infection, Immunology and Inflammation, Vanderbilt University Medical Center, Nashville, Tennessee, United States*

Complete contact information is available at: https://pubs.acs.org/10.1021/acsinfecdis.0c00500

Author Contributions

‖(J.P.D. and K.M.A.) These authors contributed equally.

Notes

The authors declare no competing financial interest.

■ ACKNOWLEDGMENTS

We thank the members of the Plate group for a critical reading of the manuscript. This work was funded by T32 AI112541 and the National Science Foundation Graduate Research Fellowship Program (1937963, K.M.A.); T32 GM008554

(J.P.D.), T32 GM065086 (E.F.M.), NIGMS R35 award (R35 GM133552), as well as Vanderbilt University startup funds.

REFERENCES

(1) Fehr, A. R., and Perlman, S. (2015) Coronaviruses: An Overview of Their Replication and Pathogenesis. *Methods Mol. Biol. 1282*, 1.
(2) *Novel Coronavirus (2019-NCoV) Situation Report 1*; World Health Organization; 2020. Online at https://apps.who.int/iris/handle/10665/330760 (accessed July 1, 2020).
(3) Hoffmann, M., Kleine-Weber, H., Schroeder, S., Müller, M. A., Drosten, C., Pöhlmann, S., et al. (2020) SARS-CoV-2 Cell Entry Depends on ACE2 and TMPRSS2 and Is Blocked by a Clinically Proven Protease Inhibitor. *Cell 181*, 271−280.
(4) Perlman, S., and Netland, J. (2009) Coronaviruses Post-SARS: Update on Replication and Pathogenesis. *Nat. Rev. Microbiol. 7*, 439−450.
(5) Blanco-Melo, D., Nilsson-Payant, B. E., Liu, W.-C., Uhl, S., Hoagland, D., Møller, R., Jordan, T. X., Oishi, K., Panis, M., Sachs, D., Wang, T. T., Schwartz, R. E., Lim, J. K., Albrecht, R. A., and TenOever, B. R. (2020) Imbalanced Host Response to SARS-CoV-2 Drives Development of COVID-19. *Cell 181* (5), 1036−1045e9.
(6) Fung, T. S., and Liu, D. X. (2014) Coronavirus Infection, ER Stress, Apoptosis and Innate Immunity. *Front. Microbiol. 5*, 296.
(7) Tan, Y.-X., Tan, T. H. P., Lee, M. J.-R., Tham, P.-Y., Gunalan, V., Druce, J., Birch, C., Catton, M., Fu, N. Y., Yu, V. C., and Tan, Y.-J. (2007) Induction of Apoptosis by the Severe Acute Respiratory Syndrome Coronavirus 7a Protein Is Dependent on Its Interaction with the Bcl-XL Protein. *J. Virol. 81* (12), 6346−6355.
(8) Yeung, M. L., Yao, Y., Jia, L., Chan, J. F. W., Chan, K. H., Cheung, K. F., Chen, H., Poon, V. K. M., Tsang, A. K. L., To, K. K. W., Yiu, M. K., Teng, J. L. L., Chu, H., Zhou, J., Zhang, Q., Deng, W., Lau, S. K. P., Lau, J. Y. N., Woo, P. C. Y., Chan, T. M., Yung, S., Zheng, B. J., Jin, D. Y., Mathieson, P. W., Qin, C., and Yuen, K. Y. (2016) MERS Coronavirus Induces Apoptosis in Kidney and Lung by Upregulating Smad7 and FGF2. *Nat. Microbiol. 1* (3), 1−8.
(9) Yue, Y., Nabar, N. R., Shi, C. S., Kamenyeva, O., Xiao, X., Hwang, I. Y., Wang, M., and Kehrl, J. H. (2018) SARS-Coronavirus Open Reading Frame-3a Drives Multimodal Necrotic Cell Death. *Cell Death Dis. 9* (9), 1−15.
(10) von Brunn, A., Teepe, C., Simpson, J. C., Pepperkok, R., Friedel, C. C., Zimmer, R., Roberts, R., Baric, R., and Haas, J. (2007) Analysis of Intraviral Protein-Protein Interactions of the SARS Coronavirus ORFeome. *PLoS One 2* (5), e459.
(11) Pfefferle, S., Schöpf, J., Kögl, M., Friedel, C. C., Müller, M. A., Carbajo-Lozoya, J., Stellberger, T., von Dall'Armi, E., Herzog, P., Kallies, S., Niemeyer, D., Ditt, V., Kuri, T., Züst, R., Pumpor, K., Hilgenfeld, R., Schwarz, F., Zimmer, R., Steffen, I., Weber, F., Thiel, V., Herrler, G., Thiel, H.-J., Schwegmann-Weßels, C., Pöhlmann, S., Haas, J., Drosten, C., and von Brunn, A. (2011) The SARS-Coronavirus-Host Interactome: Identification of Cyclophilins as Target for Pan-Coronavirus Inhibitors. *PLoS Pathog. 7* (10), e1002331.
(12) V'kovski, P., Gerber, M., Kelly, J., Pfaender, S., Ebert, N., Braga Lagache, S., Simillion, C., Portmann, J., Stalder, H., Gaschen, V., Bruggmann, R., Stoffel, M. H., Heller, M., Dijkman, R., and Thiel, V. (2019) Determination of Host Proteins Composing the Microenvironment of Coronavirus Replicase Complexes by Proximity-Labeling. *eLife 8*, No. e42037.
(13) Jean Beltran, P. M., Cook, K. C., and Cristea, I. M. (2017) Exploring and Exploiting Proteome Organization during Viral Infection. *J. Virol. 91* (18), e00268−17.
(14) Hashimoto, Y., Sheng, X., Murray-Nerger, L. A., and Cristea, I. M. (2020) Temporal Dynamics of Protein Complex Formation and Dissociation during Human Cytomegalovirus Infection. *Nat. Commun. 11* (1), 806.
(15) Shah, P. S., Link, N., Jang, G. M., Sharp, P. P., Zhu, T., Swaney, D. L., Johnson, J. R., Von Dollen, J., Ramage, H. R., Satkamp, L., Newton, B., Hüttenhain, R., Petit, M. J., Baum, T., Everitt, A., Laufman, O., Tassetto, M., Shales, M., Stevenson, E., Iglesias, G. N., Shokat, L., Tripathi, S., Balasubramaniam, V., Webb, L. G., Aguirre, S., Willsey, A. J., Garcia-Sastre, A., Pollard, K. S., Cherry, S., Gamarnik, A. V., Marazzi, I., Taunton, J., Fernandez-Sesma, A., Bellen, H. J., Andino, R., and Krogan, N. J. (2018) Comparative Flavivirus-Host Protein Interaction Mapping Reveals Mechanisms of Dengue and Zika Virus Pathogenesis. *Cell 175* (7), 1931−1945e18.
(16) Nicod, C., Banaei-Esfahani, A., and Collins, B. C. (2017) Elucidation of Host−Pathogen Protein−Protein Interactions to Uncover Mechanisms of Host Cell Rewiring. *Curr. Opin. Microbiol. 39*, 7−15.
(17) Cornillez-Ty, C. T., Liao, L., Yates, J. R., III, Kuhn, P., and Buchmeier, M. J. (2009) Severe Acute Respiratory Syndrome Coronavirus Nonstructural Protein 2 Interacts with a Host Protein Complex Involved in Mitochondrial Biogenesis and Intracellular Signaling. *J. Virol. 83* (19), 10314.
(18) Gordon, D. E., Jang, G. M., Bouhaddou, M., Xu, J., Obernier, K., White, K. M., O'Meara, M. J., Rezelj, V. V., Guo, J. Z., Swaney, D. L., Tummino, T. A., Hüttenhain, R., Kaake, R. M., Richards, A. L., Tutuncuoglu, B., Foussard, H., Batra, J., Haas, K., Modak, M., Kim, M., Haas, P., Polacco, B. J., Braberg, H., Fabius, J. M., Eckhardt, M., Soucheray, M., Bennett, M. J., Cakir, M., McGregor, M. J., Li, Q., Meyer, B., Roesch, F., Vallet, T., Mac Kain, A., Miorin, L., Moreno, E., Naing, Z. Z. C., Zhou, Y., Peng, S., Shi, Y., Zhang, Z., Shen, W., Kirby, I. T., Melnyk, J. E., Chorba, J. S., Lou, K., Dai, S. A., Barrio-Hernandez, I., Memon, D., Hernandez-Armenta, C., Lyu, J., Mathy, C. J. P., Perica, T., Pilla, K. B., Ganesan, S. J., Saltzberg, D. J., Rakesh, R., Liu, X., Rosenthal, S. B., Calviello, L., Venkataramanan, S., Liboy-Lugo, J., Lin, Y., Huang, X.-P., Liu, Y., Wankowicz, S. A., Bohn, M., Safari, M., Ugur, F. S., Koh, C., Savar, N. S., Tran, Q. D., Shengjuler, D., Fletcher, S. J., O'Neal, M. C., Cai, Y., Chang, J. C. J., Broadhurst, D. J., Klippsten, S., Sharp, P. P., Wenzell, N. A., Kuzuoglu-Ozturk, D., Wang, H.-Y., Trenker, R., Young, J. M., Cavero, D. A., Hiatt, J., Roth, T. L., Rathore, U., Subramanian, A., Noack, J., Hubert, M., Stroud, R. M., Frankel, A. D., Rosenberg, O. S., Verba, K. A., Agard, D. A., Ott, M., Emerman, M., Jura, N., von Zastrow, M., Verdin, E., Ashworth, A., Schwartz, O., D'Enfert, C., Mukherjee, S., Jacobson, M., Malik, H. S., Fujimori, D. G., Ideker, T., Craik, C. S., Floor, S. N., Fraser, J. S., Gross, J. D., Sali, A., Roth, B. L., Ruggero, D., Taunton, J., Kortemme, T., Beltrao, P., Vignuzzi, M., García-Sastre, A., Shokat, K. M., Shoichet, B. K., and Krogan, N. J. (2020) A SARS-CoV-2 Protein Interaction Map Reveals Targets for Drug Repurposing. *Nature 583* (7816), 459−468.
(19) Brito, A. F., and Pinney, J. W. (2017) Protein-Protein Interactions in Virus-Host Systems. *Front. Microbiol. 8*, 1557.
(20) Graham, R. L., Sims, A. C., Brockway, S. M., Baric, R. S., and Denison, M. R. (2005) The Nsp2 Replicase Proteins of Murine Hepatitis Virus and Severe Acute Respiratory Syndrome Coronavirus Are Dispensable for Viral Replication. *J. Virol. 79* (21), 13399−13411.
(21) Angeletti, S., Benvenuto, D., Bianchi, M., Giovanetti, M., Pascarella, S., and Ciccozzi, M. (2020) COVID-2019: The Role of the Nsp2 and Nsp3 in Its Pathogenesis. *J. Med. Virol. 92* (6), 584−588.
(22) Oostra, M., te Lintelo, E. G., Deijs, M., Verheije, M. H., Rottier, P. J. M., and de Haan, C. A. M. (2007) Localization and Membrane Topology of Coronavirus Nonstructural Protein 4: Involvement of the Early Secretory Pathway in Replication. *J. Virol. 81* (22), 12323−12336.
(23) Gadlage, M. J., Sparks, J. S., Beachboard, D. C., Cox, R. G., Doyle, J. D., Stobart, C. C., and Denison, M. R. (2010) Murine Hepatitis Virus Nonstructural Protein 4 Regulates Virus-Induced Membrane Modifications and Replication Complex Function. *J. Virol. 84* (1), 280−290.
(24) Oudshoorn, D., Rijs, K., Limpens, R. W. A. L., Groen, K., Koster, A. J., Snijder, E. J., Kikkert, M., and Bárcena, M. (2017) Expression and Cleavage of Middle East Respiratory Syndrome Coronavirus Nsp3−4 Polyprotein Induce the Formation of Double-Membrane Vesicles That Mimic Those Associated with Coronaviral RNA Replication. *mBio 8* (6), e01658−17.

(25) Kanjanahaluethai, A., Chen, Z., Jukneliene, D., and Baker, S. C. (2007) Membrane Topology of Murine Coronavirus Replicase Nonstructural Protein 3. *Virology 361* (2), 391−401.
(26) Nusinow, D. P., Szpyt, J., Ghandi, M., Rose, C. M., McDonald, E. R., Kalocsay, M., Jané-Valbuena, J., Gelfand, E., Schweppe, D. K., Jedrychowski, M., Golji, J., Porter, D. A., Rejtar, T., Wang, Y. K., Kryukov, G. V., Stegmeier, F., Erickson, B. K., Garraway, L. A., Sellers, W. R., and Gygi, S. P. (2020) Quantitative Proteomics of the Cancer Cell Line Encyclopedia. *Cell 180* (2), 387−402e16.
(27) Jiang, L., Wang, M., Lin, S., Jian, R., Li, X., Chan, J., Dong, G., Fang, H., Robinson, A. E., Aguet, F., Anand, S., Ardlie, K. G., Gabriel, S., Getz, G., Graubert, A., Hadley, K., Handsaker, R. E., Huang, K. H., Kashin, S., MacArthur, D. G., Meier, S. R., Nedzel, J. L., Nguyen, D. Y., Segrè, A. V., Todres, E., Balliu, B., Barbeira, A. N., Battle, A., Bonazzola, R., Brown, A., Brown, C. D., Castel, S. E., Conrad, D., Cotter, D. J., Cox, N., Das, S., de Goede, O. M., Dermitzakis, E. T., Engelhardt, B. E., Eskin, E., Eulalio, T. Y., Ferraro, N. M., Flynn, E., Fresard, L., Gamazon, E. R., Garrido-Martín, D., Gay, N. R., Guigó, R., Hamel, A. R., He, Y., Hoffman, P. J., Hormozdiari, F., Hou, L., Im, H. K., Jo, B., Kasela, S., Kellis, M., Kim-Hellmuth, S., Kwong, A., Lappalainen, T., Li, X., Liang, Y., Mangul, S., Mohammadi, P., Montgomery, S. B., Muñoz-Aguirre, M., Nachun, D. C., Nobel, A. B., Oliva, M., Park, Y. S., Park, Y., Parsana, P., Reverter, F., Rouhana, J. M., Sabatti, C., Saha, A., Skol, A. D., Stephens, M., Stranger, B. E., Strober, B. J., Teran, N. A., Viñuela, A., Wang, G., Wen, X., Wright, F., Wucher, V., Zou, Y., Ferreira, P. G., Li, G., Melé, M., Yeger-Lotem, E., Barcus, M. E., Bradbury, D., Krubit, T., McLean, J. A., Qi, L., Robinson, K., Roche, N. V., Smith, A. M., Sobin, L., Tabor, D. E., Undale, A., Bridge, J., Brigham, L. E., Foster, B. A., Gillard, B. M., Hasz, R., Hunter, M., Johns, C., Johnson, M., Karasik, E., Kopen, G., Leinweber, W. F., McDonald, A., Moser, M. T., Myer, K., Ramsey, K. D., Roe, B., Shad, S., Thomas, J. A., Walters, G., Washington, M., Wheeler, J., Jewell, S. D., Rohrer, D. C., Valley, D. R., Davis, D. A., Mash, D. C., Branton, P. A., Barker, L. K., Gardiner, H. M., Mosavel, M., Siminoff, L. A., Flicek, P., Haeussler, M., Juettemann, T., Kent, W. J., Lee, C. M., Powell, C. C., Rosenbloom, K. R., Ruffier, M., Sheppard, D., Taylor, K., Trevanion, S. J., Zerbino, D. R., Abell, N. S., Akey, J., Chen, L., Demanelis, K., Doherty, J. A., Feinberg, A. P., Hansen, K. D., Hickey, P. F., Jasmine, F., Kaul, R., Kibriya, M. G., Li, J. B., Li, Q., Linder, S. E., Pierce, B. L., Rizzardi, L. F., Smith, K. S., Stamatoyannopoulos, J., Tang, H., Carithers, L. J., Guan, P., Koester, S. E., Little, A. R., Moore, H. M., Nierras, C. R., Rao, A. K., Vaught, J. B., Volpi, S., and Snyder, M. P. (2020) A Quantitative Proteome Map of the Human Body. *Cell 183* (1), 269−283e19.
(28) Wang, D., Eraslan, B., Wieland, T., Hallström, B., Hopf, T., Zolg, D. P., Zecha, J., Asplund, A., Li, L., Meng, C., Frejno, M., Schmidt, T., Schnatbaum, K., Wilhelm, M., Ponten, F., Uhlen, M., Gagneur, J., Hahne, H., and Kuster, B. A. (2019) Deep Proteome and Transcriptome Abundance Atlas of 29 Healthy Human Tissues. *Mol. Syst. Biol. 15* (2), e8503.
(29) Christie, D. A., Lemke, C. D., Elias, I. M., Chau, L. A., Kirchhof, M. G., Li, B., Ball, E. H., Dunn, S. D., Hatch, G. M., and Madrenas, J. (2011) Stomatin-Like Protein 2 Binds Cardiolipin and Regulates Mitochondrial Biogenesis and Function. *Mol. Cell. Biol. 31* (18), 3845−3856.
(30) Panda, D., Gold, B., Tartell, M. A., Rausch, K., Casas-Tinto, S., and Cherry, S. (2015) The Transcription Factor FoxK Participates with Nup98 to Regulate Antiviral Gene Expression. *mBio 6* (2), e02509−14.
(31) Yenamandra, S. P., Lundin, A., Arulampalam, V., Yurchenko, M., Pettersson, S., Klein, G., and Kashuba, E. (2009) Expression Profile of Nuclear Receptors upon Epstein – Barr Virus Induced B Cell Transformation. *Exp. Oncol. 31* (2), 92−96.
(32) Gavin, A. L., Huang, D., Huber, C., Mårtensson, A., Tardif, V., Skog, P. D., Blane, T. R., Thinnes, T. C., Osborn, K., Chong, H. S., Kargaran, F., Kimm, P., Zeitjian, A., Sielski, R. L., Briggs, M., Schulz, S. R., Zarpellon, A., Cravatt, B., Pang, E. S., Teijaro, J., de la Torre, J. C., O'Keeffe, M., Hochrein, H., Damme, M., Teyton, L., Lawson, B. R., and Nemazee, D. (2018) PLD3 and PLD4 Are Single-Stranded Acid Exonucleases That Regulate Endosomal Nucleic-Acid Sensing. *Nat. Immunol. 19* (9), 942−953.
(33) Parks, C. L., and Shenk, T. (1997) Activation of the Adenovirus Major Late Promoter by Transcription Factors MAZ and Sp1. *J. Virol. 71* (12), 9600−9607.
(34) Ovsyannikova, I. G., Salk, H. M., Kennedy, R. B., Haralambieva, I. H., Zimmermann, M. T., Grill, D. E., Oberg, A. L., and Poland, G. A. (2016) Gene Signatures Associated with Adaptive Humoral Immunity Following Seasonal Influenza A/H1N1 Vaccination. *Genes Immun. 17* (7), 371−379.
(35) Le, M. X., Haddad, D., Ling, A. K., Li, C., So, C. C., Chopra, A., Hu, R., Angulo, J. F., Moffat, J., and Martin, A. (2016) Kin17 Facilitates Multiple Double-Strand Break Repair Pathways That Govern B Cell Class Switching. *Sci. Rep. 6* (1), 37215.
(36) Zhong, B., Zhang, L., Lei, C., Li, Y., Mao, A. P., Yang, Y., Wang, Y. Y., Zhang, X. L., and Shu, H. B. (2009) The Ubiquitin Ligase RNF5 Regulates Antiviral Responses by Mediating Degradation of the Adaptor Protein MITA. *Immunity 30* (3), 397−407.
(37) Fenech, E. J., Lari, F., Charles, P. D., Fischer, R., Laétitia-Thézénas, M., Bagola, K., Paton, A. W., Paton, J. C., Gyrd-Hansen, M., Kessler, B. M., and Christianson, J. C. (2020) Interaction Mapping of Endoplasmic Reticulum Ubiquitin Ligases Identifies Modulators of Innate Immune Signalling. *eLife 9*, No. e57306.
(38) Owen, R. P., Gong, L., Sagreiya, H., Klein, T. E., and Altman, R. B. (2010) VKORC1 Pharmacogenomics Summary. *Pharmacogenet. Genomics 20* (10), 642−644.
(39) Ho, D. V., and Chan, J. Y. (2015) Induction of Herpud1 Expression by ER Stress Is Regulated by Nrf1. *FEBS Lett. 589* (5), 615−620.
(40) Qin, L., Guo, J., Zheng, Q., and Zhang, H. (2016) BAG2 Structure, Function and Involvement in Disease. *Cell. Mol. Biol. Lett. 21* (1), 18.
(41) Chartron, J. W., Suloway, C. J. M., Zaslaver, M., and Clemons, W. M. (2010) Structural Characterization of the Get4/Get5 Complex and Its Interaction with Get3. *Proc. Natl. Acad. Sci. U. S. A. 107* (27), 12127−12132.
(42) Gottier, P., Gonzalez-Salgado, A., Menon, A. K., Liu, Y. C., Acosta-Serrano, A., and Bütikofer, P. (2017) RFT1 Protein Affects Glycosylphosphatidylinositol (GPI) Anchor Glycosylation. *J. Biol. Chem. 292* (3), 1103−1111.
(43) Haeuptle, M. A., Pujol, F. M., Neupert, C., Winchester, B., Kastaniotis, A. J. J., Aebi, M., and Hennet, T. (2008) Human RFT1 Deficiency Leads to a Disorder of N-Linked Glycosylation. *Am. J. Hum. Genet. 82* (3), 600−606.
(44) Papp, B., Brouland, J.-P., Arbabian, A., Gélébart, P., Kovács, T., Bobe, R., Enouf, J., Varin-Blank, N., and Apáti, Á. (2012) Endoplasmic Reticulum Calcium Pumps and Cancer Cell Differentiation. *Biomolecules 2* (1), 165−186.
(45) Seo, J., Lee, S. H., Park, S. Y., Jeong, M. H., Lee, S. Y., Kim, M. J., Yoo, J. Y., Jang, S., Choi, K. C., and Yoon, Ho G. (2019) GPR177 Promotes Gastric Cancer Proliferation by Suppressing Endoplasmic Reticulum Stress-Induced Cell Death. *J. Cell. Biochem. 120* (2), 2532−2539.
(46) Cui, J., Chen, W., Sun, J., Guo, H., Madley, R., Xiong, Y., Pan, X., Wang, H., Tai, A. W., Weiss, M. A., Arvan, P., and Liu, M. (2015) Competitive Inhibition of the Endoplasmic Reticulum Signal Peptidase by Non-Cleavable Mutant Preprotein Cargos. *J. Biol. Chem. 290* (47), 28131−28140.
(47) Blanc, M., Hsieh, W. Y., Robertson, K. A., Watterson, S., Shui, G., Lacaze, P., Khondoker, M., Dickinson, P., Sing, G., Rodríguez-Martín, S., Phelan, P., Forster, T., Strobl, B., Müller, M., Riemersma, R., Osborne, T., Wenk, M. R., Angulo, A., and Ghazal, P. (2011) Host Defense against Viral Infection Involves Interferon Mediated Down-Regulation of Sterol Biosynthesis. *PLoS Biol. 9* (3), e1000598.
(48) van 't Wout, A. B., Swain, J. V., Schindler, M., Rao, U., Pathmajeyan, M. S., Mullins, J. I., and Kirchhoff, F. (2005) Nef Induces Multiple Genes Involved in Cholesterol Synthesis and Uptake in Human Immunodeficiency Virus Type 1-Infected T Cells. *J. Virol. 79* (15), 10053−10058.

https://dx.doi.org/10.1021/acsinfecdis.0c00500
ACS Infect. Dis. 2020, 6, 3174−3189

(49) Diamond, D. L., Syder, A. J., Jacobs, J. M., Sorensen, C. M., Walters, K.-A., Proll, S. C., McDermott, J. E., Gritsenko, M. A., Zhang, Q., Zhao, R., Metz, T. O., Camp, D. G., Waters, K. M., Smith, R. D., Rice, C. M., and Katze, M. G. (2010) Temporal Proteome and Lipidome Profiles Reveal Hepatitis C Virus-Associated Reprogramming of Hepatocellular Metabolism and Bioenergetics. *PLoS Pathog. 6* (1), e1000719.

(50) Xiao, J., Li, W., Zheng, X., Qi, L., Wang, H., Zhang, C., Wan, X., Zheng, Y., Zhong, R., Zhou, X., Lu, Y., Li, Z., Qiu, Y., Liu, C., Zhang, F., Zhang, Y., Xu, X., Yang, Z., Chen, H., Zhai, Q., Wei, B., and Wang, H. (2020) Targeting 7-Dehydrocholesterol Reductase Integrates Cholesterol Metabolism and IRF3 Activation to Eliminate Infection. *Immunity 52* (1), 109−122e6.

(51) Larance, M., Kirkwood, K. J., Xirodimas, D. P., Lundberg, E., Uhlen, M., and Lamond, A. I. (2012) Characterization of MRFAP1 Turnover and Interactions Downstream of the NEDD8 Pathway. *Mol. Cell. Proteomics 11* (3), M111014407.

(52) Kelly, T. J., Suzuki, H. I., Zamudio, J. R., Suzuki, M., and Sharp, P. A. (2019) Sequestration of MicroRNA-Mediated Target Repression by the Ago2-Associated RNA-Binding Protein FAM120A. *RNA 25* (10), 1291−1297.

(53) Bartolomé, R. A., García-Palmero, I., Torres, S., López-Lucendo, M., Balyasnikova, I. V., and Casal, J. I. (2015) IL13 Receptor A2 Signaling Requires a Scaffold Protein, FAM120A, to Activate the FAK and PI3K Pathways in Colon Cancer Metastasis. *Cancer Res. 75* (12), 2434−2444.

(54) Lampert, F., Stafa, D., Goga, A., Soste, M. V., Gilberto, S., Olieric, N., Picotti, P., Stoffel, M., and Peter, M. (2018) The Multi-Subunit GID/CTLH E3 Ubiquitin Ligase Promotes Cell Proliferation and Targets the Transcription Factor Hbp1 for Degradation. *eLife 7*, No. e35528.

(55) Cho, K. F., Branon, T. C., Rajeev, S., Svinkina, T., Udeshi, N. D., Thoudam, T., Kwak, C., Rhee, H.-W., Lee, I.-K., Carr, S. A., and Ting, A. Y. (2020) Split-TurboID Enables Contact-Dependent Proximity Labeling in Cells. *Proc. Natl. Acad. Sci. U. S. A. 117* (22), 12143−12154.

(56) Kwak, C., Shin, S., Park, J.-S., Jung, M., Nhung, T. T. M., Kang, M.-G., Lee, C., Kwon, T.-H., Park, S. K., Mun, J. Y., Kim, J.-S., and Rhee, H.-W. (2020) Contact-ID, a Tool for Profiling Organelle Contact Sites, Reveals Regulatory Proteins of Mitochondrial-Associated Membrane Formation. *Proc. Natl. Acad. Sci. U. S. A. 117* (22), 12109−12120.

(57) Carreras-Sureda, A., Jaña, F., Urra, H., Durand, S., Mortenson, D. E., Sagredo, A., Bustos, G., Hazari, Y., Ramos-Fernández, E., Sassano, M. L., Pihán, P., van Vliet, A. R., González-Quiroz, M., Torres, A. K., Tapia-Rojas, C., Kerkhofs, M., Vicente, R., Kaufman, R. J., Inestrosa, N. C., Gonzalez-Billault, C., Wiseman, R. L., Agostinis, P., Bultynck, G., Court, F. A., Kroemer, G., Cárdenas, J. C., and Hetz, C. (2019) Non-Canonical Function of IRE1α Determines Mitochondria-Associated Endoplasmic Reticulum Composition to Control Calcium Transfer and Bioenergetics. *Nat. Cell Biol. 21* (6), 755−767.

(58) Kim, J. H., Rhee, J. K., Ahn, D. G., Kim, K. P., and Oh, J. W. (2014) Interaction of Stomatin with Hepatitis C Virus RNA Polymerase Stabilizes the Viral RNA Replicase Complexes on Detergent-Resistant Membranes. *J. Microbiol. Biotechnol. 24* (12), 1744−1754.

(59) Wintachai, P., Wikan, N., Kuadkitkan, A., Jaimipuk, T., Ubol, S., Pulmanausahakul, R., Auewarakul, P., Kasinrerk, W., Weng, W. Y., Panyasrivanit, M., Paemanee, A., Kittisenachai, S., Roytrakul, S., and Smith, D. R. (2012) Identification of Prohibitin as a Chikungunya Virus Receptor Protein. *J. Med. Virol. 84* (11), 1757−1770.

(60) Too, I. H. K., Bonne, I., Tan, E. L., Chu, J. J. H., and Alonso, S. (2018) Prohibitin Plays a Critical Role in Enterovirus 71 Neuropathogenesis. *PLoS Pathog. 14* (1), e1006778.

(61) Richter, K. T., Kschonsak, Y. T., Vodicska, B., and Hoffmann, I. (2020) FBXO45-MYCBP2 Regulates Mitotic Cell Fate by Targeting FBXW7 for Degradation. *Cell Death Differ. 27* (2), 758−772.

(62) Gordon, D. E., Hiatt, J., Bouhaddou, M., Rezelj, V. V., Ulferts, S., Braberg, H., Jureka, A. S., Obernier, K., Guo, J. Z., Batra, J., Kaake, R. M., Weckstein, A. R., Owens, T. W., Gupta, M., Pourmal, S., Titus, E. W., Cakir, M., Soucheray, M., McGregor, M., Cakir, Z., Jang, G., O'Meara, M. J., Tummino, T. A., Zhang, Z., Foussard, H., Rojc, A., Zhou, Y., Kuchenov, D., Huttenhain, R., Xu, J., Eckhardt, M., Swaney, D. L., Fabius, J. M., Ummadi, M., Tutuncuoglu, B., Rathore, U., Modak, M., Haas, P., Haas, K. M., Naing, Z. Z. C., Pulido, E. H., Shi, Y., Barrio-Hernandez, I., Memon, D., Petsalaki, E., Dunham, A., Marrero, M. C., Burke, D., Koh, C., Vallet, T., Silvas, J. A., Azumaya, C. M., Billesbølle, C., Brilot, A. F., Campbell, M. G., Diallo, A., Dickinson, M. S., Diwanji, D., Herrera, N., Hoppe, N., Kratochvil, H. T., Liu, Y., Merz, G. E., Moritz, M., Nguyen, H. C., Nowotny, C., Puchades, C., Rizo, A. N., Schulze-Gahmen, U., Smith, A. M., Sun, M., Young, I. D., Zhao, J., Asarnow, D., Biel, J., Bowen, A., Braxton, J. R., Chen, J., Chio, C. M., Chio, U. S., Deshpande, I., Doan, L., Faust, B., Flores, S., Jin, M., Kim, K., Lam, V. L., Li, F., Li, J., Li, Y.-L., Li, Y., Liu, X., Lo, M., Lopez, K. E., Melo, A. A., Moss, F. R., Nguyen, P., Paulino, J., Pawar, K. I., Peters, J. K., Pospiech, T. H., Safari, M., Sangwan, S., Schaefer, K., Thomas, P. V., Thwin, A. C., Trenker, R., Tse, E., Tsui, T. K. M., Wang, F., Whitis, N., Yu, Z., Zhang, K., Zhang, Y., Zhou, F., Saltzberg, D., QCRG Structural Biology Consortium, Hodder, A. J., Shun-Shion, A. S., Williams, D. M., White, K. M., Rosales, R., Kehrer, T., Miorin, L., Moreno, E., Patel, A. H., Rihn, S., Khalid, M. M., Vallejo-Gracia, A., Fozouni, P., Simoneau, C. R., Roth, T. L., Wu, D., Karim, M. A., Ghoussaini, M., Dunham, I., Berardi, F., Weigang, S., Chazal, M., Park, J., Logue, J., McGrath, M., Weston, S., Haupt, R., Hastie, C. J., Elliott, M., Brown, F., Burness, K. A., Reid, E., Dorward, M., Johnson, C., Wilkinson, S. G., Geyer, A., Giesel, D. M., Baillie, C., Raggett, S., Leech, H., Toth, R., Goodman, N., Keough, K. C., Lind, A. L., Klesh, R. J., Zoonomia Consortium, Hemphill, K. R., Carlson-Stevermer, J., Oki, J., Holden, K., Maures, T., Pollard, K. S., Sali, A., Agard, D. A., Cheng, Y., Fraser, J. S., Frost, A., Jura, N., Kortemme, T., Manglik, A., Southworth, D. R., Stroud, R. M., Alessi, D. R., Davies, P., Frieman, M. B., Ideker, T., Abate, C., Jouvenet, N., Kochs, G., Shoichet, B., Ott, M., Palmarini, M., Shokat, K. M., Garcia-Sastre, A., Rassen, J. A., Grosse, R., Rosenberg, O. S., Verba, K. A., Basler, C. F., Vignuzzi, M., Peden, A. A., Beltrao, P., and Krogan, N. J. (2020) Comparative Host-Coronavirus Protein Interaction Networks Reveal Pan-Viral Disease Mechanisms. *Science (Washington, DC, U. S.) 22*, eabe9403.

(63) Heaton, B. E., Trimarco, J. D., Hamele, C. E., Harding, A. T., Tata, A., Zhu, X., Tata, P. R., Smith, C. M., and Heaton, N. S. SRSF Protein Kinases 1 and 2 Are Essential Host Factors for Human Coronaviruses Including SARS-CoV-2. *bioRxiv* 2020 DOI: 10.1101/2020.08.14.251207.

(64) Abbas, Y. M., Wu, D., Bueler, S. A., Robinson, C. V., and Rubinstein, J. L. (2020) Structure of V-ATPase from the Mammalian Brain. *Science (Washington, DC, U. S.) 367* (6483), 1240−1246.

(65) Song, X., Liu, S., Wang, W., Ma, Z., Cao, X., and Jiang, M. (2020) E3 Ubiquitin Ligase RNF170 Inhibits Innate Immune Responses by Targeting and Degrading TLR3 in Murine Cells. *Cell. Mol. Immunol. 17* (8), 865−874.

(66) Lu, J. P., Wang, Y., Sliter, D. A., Pearce, M. M. P., and Wojcikiewicz, R. J. H. (2011) RNF170 Protein, an Endoplasmic Reticulum Membrane Ubiquitin Ligase, Mediates Inositol 1,4,5-Trisphosphate Receptor Ubiquitination and Degradation. *J. Biol. Chem. 286* (27), 24426−24433.

(67) Berridge, M. J. (1993) Inositol Trisphosphate and Calcium Signalling. *Nature 361* (6410), 315−325.

(68) Bartok, A., Weaver, D., Golenár, T., Nichtova, Z., Katona, M., Bánsághi, S., Alzayady, K. J., Thomas, V. K., Ando, H., Mikoshiba, K., Joseph, S. K., Yule, D. I., Csordás, G., and Hajnóczky, G. (2019) IP3 Receptor Isoforms Differently Regulate ER-Mitochondrial Contacts and Local Calcium Transfer. *Nat. Commun. 10* (1), 1−14.

(69) Missiroli, S., Patergnani, S., Caroccia, N., Pedriali, G., Perrone, M., Previati, M., Wieckowski, M. R., and Giorgi, C. (2018) Mitochondria-Associated Membranes (MAMs) and Inflammation. *Cell Death Dis. 9* (3), 329.

(70) Kuchay, S., Saeed, M., Giorgi, C., Li, J., Hoffmann, H. H., Pinton, P., Rice, C. M., and Pagano, M. (2018) NS5A Promotes

Constitutive Degradation of IP3R3 to Counteract Apoptosis Induced by Hepatitis C Virus. *Cell Rep. 25* (4), 833−840e3.
(71) Nieto-Torres, J. L., Verdiá-Báguena, C., Jimenez-Guardeño, J. M., Regla-Nava, J. A., Castaño-Rodriguez, C., Fernandez-Delgado, R., Torres, J., Aguilella, V. M., and Enjuanes, L. (2015) Severe Acute Respiratory Syndrome Coronavirus E Protein Transports Calcium Ions and Activates the NLRP3 Inflammasome. *Virology 485*, 330−339.
(72) Bojkova, D., Klann, K., Koch, B., Widera, M., Krause, D., Ciesek, S., Cinatl, J., and Münch, C. (2020) Proteomics of SARS-CoV-2-Infected Host Cells Reveals Therapy Targets. *Nature 583* (7816), 469−472.
(73) Wright, M. T., Kouba, L., and Plate, L. Thyroglobulin Interactome Profiling Defines Altered Proteostasis Topology Associated with Thyroid Dyshormonogenesis. *Mol. Cell. Proteomics* 2020 DOI: 10.1101/2020.04.08.032482.
(74) Fonslow, B. R., Niessen, S. M., Singh, M., Wong, C. C., Xu, T., Carvalho, P. C., Choi, J., Park, S. K., and Yates, J. R., 3rd (2012) Single-Step Inline Hydroxyapatite Enrichment Facilitates Identification and Quantitation of Phosphopeptides from Mass-Limited Proteomes with MudPIT. *J. Proteome Res. 11* (5), 2697−2709.
(75) Keilhauer, E. C., Hein, M. Y., and Mann, M. (2015) Accurate Protein Complex Retrieval by Affinity Enrichment Mass Spectrometry (AE-MS) Rather than Affinity Purification Mass Spectrometry (AP-MS). *Mol. Cell. Proteomics 14* (1), 120−135.
(76) Perez-Riverol, Y., Csordas, A., Bai, J., Bernal-Llinares, M., Hewapathirana, S., Kundu, D. J., Inuganti, A., Griss, J., Mayer, G., Eisenacher, M., Pérez, E., Uszkoreit, J., Pfeuffer, J., Sachsenberg, T., Yilmaz, Ş., Tiwary, S., Cox, J., Audain, E., Walzer, M., Jarnuczak, A. F., Ternent, T., Brazma, A., and Vizcaíno, J. A. (2019) The PRIDE Database and Related Tools and Resources in 2019: Improving Support for Quantification Data. *Nucleic Acids Res. 47* (D1), D442−D450.
(77) Kuleshov, M. V., Jones, M. R., Rouillard, A. D., Fernandez, N. F., Duan, Q., Wang, Z., Koplev, S., Jenkins, S. L., Jagodnik, K. M., Lachmann, A., McDermott, M. G., Monteiro, C. D., Gundersen, G. W., and Ma'ayan, A. (2016) Enrichr: A Comprehensive Gene Set Enrichment Analysis Web Server 2016 Update. *Nucleic Acids Res. 44* (W1), W90−W97.
(78) Bozidis, P., Williamson, C. D., and Colberg-Poley, A. M. (2007) Isolation of Endoplasmic Reticulum, Mitochondria, and Mitochondria-Associated Membrane Fractions from Transfected Cells and from Human Cytomegalovirus-Infected Primary Fibroblasts. *Curr. Protoc. Cell Biol. 37* (1), 3271−32723.

https://dx.doi.org/10.1021/acsinfecdis.0c00500
ACS Infect. Dis. 2020, 6, 3174−3189